

Study on Resonance and Symmetry of Wireless Power Transfer



By

Sabriansyah Rizqika Akbar

Supervisor: Professor Ichijo Hodaka

A thesis submitted in partial fulfillment for the degree of Doctor of Philosophy.

Department of Materials and Informatics

Interdisciplinary Graduate School of Agriculture and Engineering

UNIVERSITY OF MIYAZAKI

September 2021

Dedicated to my loving family.

My mother Ernani Hadiyati and my late father Hary Priyanto
My beloved wife Dhini, and my children Zaki, Sarah, and Karin

Abstract

Inductive Wireless Power Transfer (WPT) is a common method to deliver power wirelessly that uses pairs of coils in the primary and secondary circuits. Moreover, to increase the power delivery, the circuit compensated using additional electronics elements such as capacitors to form a symmetry WPT system. Further, many researchers use a resonance calculation to obtain the optimal operating frequency to improve power delivery. However, there might be violations of the idea of resonance calculation in practical situations. The situations occur when the WPT system becomes asymmetrical, such as in the undetermined WPT parameters or the multi-receiver WPT system. This asymmetry situation makes the resonance frequency cannot be calculated using the conventional method. Therefore, methods regarding finding the optimal frequency to obtain high power delivery need to be addressed.

The WPT system modeling is essential to find the optimal parameters from the stimulus-response. The WPT system model obtained using the circuit analysis continued by defining the state-space variables. The transfer function of the WPT system can be used to get the stimulus-response or steady-state analysis by giving the value of the parameter to the models so that the optimal operating frequency can be achieved. In practical situations, there are situations whether the parameter values are unable to be determined. Therefore, we cannot give the parameter's value to the models, and the optimal operating frequency unable to be observed through the frequency response analysis. Although it is theoretically possible to determine the optimal frequency by a wide range frequency sweep, it is practically important to spot it in a few trials of frequency. Therefore, this study proposes a frequency spotting strategy using a square wave input power signal. The method avoids a long time-consuming sweeping process with knowledge of response by square wave input. The Automatic Multiscale-based Peak Detection (AMPD) algorithm is applied to select the initial peak finding on every data sample increment iteration to further enhanced to find the set of peak patterns by calculating error parameters.

Another situation that makes the WPT system is asymmetry is whether it only compensates by primary side capacitance. It should be noticed that an additional component compensation on the symmetric WPT circuit increases the equivalent series resistance and affect the power absorbed by the load receivers. The complexity of the system will increase along with the increasing number of receivers. Thus, this study explores the WPT circuit that only compensated with the primary side capacitor in transferring high power to dual receivers. Using a single capacitor on the primary side makes the circuit lacks symmetry, so it cannot use the idea of resonance. Therefore, we propose an asymmetric multi-receivers WPT model to discover high power operating points and use an optimization approach to obtain the optimal parameters. This study challenges several design variables optimization to obtain high power operating point. The NSGA-II (Non-dominated Sorting Genetic Algorithm II) is used to optimize the mathematical system model design variables. The results show that the proposed system can obtain high power even though using only a single capacitor compensation without the idea of resonance.

This study's finding highlight is the contribution of presenting an approach to obtain the high power from an asymmetric situation that cannot use the idea of resonance. A fast-spotting strategy to find optimal frequency has been proposed in the single receivers with some indeterministic parameters. The wireless high-power transfer can be achieved in the multi-receiver WPT system even if the circuits lack symmetry. Therefore, the capacitor on the receiver side can be neglected to reduce the complexity of the receiver circuit.

This dissertation consists of 5 chapters. **Chapter 1 introduction** explains the background regarding the current situation of WPT research and the explanation of resonant (symmetry) and non-resonant (Asymmetry) situations. This chapter also presents the objective of the study, followed by the scope, contributions, and findings. **Chapter 2 Resonance and Symmetric Circuit** explains the common symmetric WPT circuit and the idea of resonance. This study observed the behavior of the symmetric WPT system by obtaining the circuit model through transfer function calculation. Afterward, the situation of the WPT system is presented in the form of frequency response and steady-state analysis. **Chapter 3 A Fast-Spotting Strategy of Optimal Frequency in Wireless Power Transfer** presenting a method to obtain the high-power delivery without using the idea of resonance using a fast frequency spotting strategy using a square wave input power signal. **Chapter 4 A Design Approach to Wireless High-Power Transfer to Multiple Receivers with Asymmetric Circuit** presents methods to obtain high-power in the asymmetric circuit. This study investigates a method to deliver high power in a circuit whether the idea of resonance is cannot be used. This section is presenting an optimization approach to obtain the optimal parameters in several design challenges. **Chapter 5 Summary** gives a summarization of studies. It concludes the results regarding the investigation of the idea of resonance and symmetric circuits continue by presenting approaches to obtain high-power without the idea of resonance or in an asymmetric circuit. Moreover, this chapter explains the future works based on the current study.

Acknowledgment

All my family, friends, colleagues, and the mentioned person on this page have a special meaning for the author's life during pursue to becoming a better and wiser person.

1. I would like to express my deepest appreciation and gratitude to my supervisor, Professor Ichijo Hodaka, as the head of Automatics Control Laboratory UoM, for invaluable guidance, encouragement, and patience. It is an honor to become his student.
2. I would like to express my gratitude to the committee, Professor Koichi Tanno, Professor Hiroki Tamura, Professor Masahiro Tasumi, and Professor Masahiro Yokomichi for their excellent advice and insight.
3. The author would like to acknowledge the invaluable support from the University of Miyazaki, especially from the interdisciplinary graduate school of agriculture and engineering, student service division, and global support office.
4. The author is highly grateful to the Rotary Yoneyama Memorial Foundation scholarship, the support and hostility from the Takanabe Rotary care club, and guidance from the Rotary counselor Mr. Ishida Yoshikatsu.
5. The author would also be grateful for MEXT and JASSO's scholarship support in the early semester of the study.
6. I would like to say thank you to the University of Brawijaya and the Faculty of Computer Science for all the support during my study.
7. The author would like to express his gratitude to parents, mother Ernani Hadiyati and the late father Hary Priyanto, and parents in law, Puji Astuti and Karimuddin for the endless caring and praying for the author and his family.
8. The author would like to express his gratitude to his loving family, wife Dhini Riezqa Arimbi, and children, Sultan Mikai Zaki Albani, Sarah Jasmin Khairunnisa, and Sabia Bilqis Khairina for giving the author unconditional love and understanding.
9. I would like to extend my sincere thanks to to my sister Sabrina Aulia Rahma and his husband Issa Arwani. Also, a special thank you to Yuniar Setiawan and his family for always supporting my family and me.
10. Thank you to all my friends Barlian H.P, Eko Setiawan, M. Chandra Setiawan, Bayu Priambadha, and their families for all the support to me and my family.
11. The author would like to acknowledge the support from the alumni laboratory members Mayu Suzuki, Hakugin Shoichiro, Ohata Takahiro, Nao Hashimoto, and Matsura Kento.
12. Thank you to the Indonesian student community for the beautiful friendship while study and enjoying living in the beautiful and mesmerizing city of Miyazaki, Japan.

Above all, the author gives his spiritual grateful to the Almighty Allah SWT to help the author accomplished this work by giving me the opportunity, health, and strength.

List of Publications

Journal Articles

Akbar, S.R. & Hodaka, I. 2020, "A fast spotting strategy of optimal frequency in wireless power transfer", International Journal of Electrical and Electronic Engineering and Telecommunications, vol. 9, no. 4, pp. 242-246.

Akbar, S.R. & Hodaka, I. 2021, "A design approach to wireless high-power transfer to multiple receivers with asymmetric circuit", International Journal of Circuits, Systems and Signal Processing, vol. 15, pp. 125-134.

Conference Proceedings:

Akbar, S.R. & Hodaka, I. 2021, "The Optimization of Dual Receiver Wireless Power Transfer", International Conference on Mathematics and Computers in Science and Engineering, MACISE 2021.

Table of Contents

Abstract	iii
Table of Contents	vii
List of Figures	ix
List of Tables	x
Chapter 1	1
Introduction	1
1.1 Background	1
1.2 Research Objectives	2
1.3 Research Scope	2
1.4 Contributions and Findings.....	3
1.5 Outline	3
Chapter 2	5
Resonance and Symmetric Circuit	5
2.1 Wireless Power Transfer Symmetric Circuit.....	5
2.2 System Model of Wireless Power Transfer.....	7
2.3 Frequency Response	8
2.4 Steady-State Analysis	9
2.5 Optimization of Power	10
Chapter 3	12
A Fast-Spotting Strategy of Optimal Frequency in Wireless Power Transfer	12
3.1 Background	12
3.2 Proposed Method	13
3.3 Result and discussion	15
3.4 Conclusions.....	19
Chapter 4	20
A Design Approach to Wireless High-Power Transfer to Multiple Receivers with Asymmetric Circuit	20
4.1 Background	20
4.2 Proposed Method	21
4.2.1 System Model	21
4.2.2 Objective function and Optimization.....	23

4.2.3 Objective Functions	24
4.2.4 Design Variables: Capacitance, Frequency, and Coupling Coefficients	24
4.2.5 Design Variables: Capacitance, Primary Coil, and Coupling Coefficients	26
4.2.6 Design Variables: Capacitance and Frequency	27
4.2.7 Optimization Tools and Decision Making	27
4.3 Results and Discussion	27
4.3.1 Optimization Results with Capacitance, Frequency, and Coupling Coefficients as Design Variables	27
4.3.2 Optimization Results with Capacitance, Primary Coil and Coupling Coefficients as Design Variables	29
4.3.3 Optimization Results with Capacitance and Frequency Design Variables	30
4.3.4 Comparison Between Proposed WPT Circuit with The Common WPT circuit.	33
4.3.5 Discussions	35
4.4 Conclusions	38
Chapter 5 Summary	39
References	41

List of Figures

Figure 1.1. Research Scope.....	3
Figure 2.1. Wireless Power Transfer.....	5
Figure 2.2. Wireless Power Transfer Symmetric Circuit	6
Figure 2.3. Frequency Response using Square Wave and Sine Wave	8
Figure 2.4. the steady-state plot of voltage ($y_{ss}(t)$) and power ($p_{ss}(t)$) in RL	9
Figure 2.5. RL Power Frequency Response of Symmetric WPT Circuit	10
Figure 2.6. Optimal Power.....	11
Figure 3.1. Transferred power to 20 Ohm load depending on the driving frequency (experiment). ..	13
Figure 3.2. Proposed Method Flowchart	14
Figure 3.3. The experiment conducted to collect e_{total} on each iteration with $d=400$. The data sample increment (i) starts with 10 kHz interval and find the e_{total} value from 5-100 kHz.....	15
Figure 3.4. The Experiment during the 159 data samples with 10 peaks found by the AMPD Algorithm.	16
Figure 3.5. The 159 data samples with set of peaks ($l = l_4, l_3, l_2, l_1, l_0$) respectively from smallest to highest frequency alongside with the peak width, after being selected by the spotting strategies	17
Figure 3.6. Three experimental data consists of 950 power data, received from WPT system by 20 Ohm resistor using square wave input signal.	18
Figure 3.7. The experiment conducted to collect e_{total} on each iteration with $d = 400$ from a total 238 of data samples in Data-2 with the $e_{total} < 0.8$ start at the 173 data samples.....	19
Figure 3.8. The experiment conducted to collect e_{total} on each iteration with $d = 400$ from a total 238 of data samples in. Data-3 with the $e_{total} < 0.8$ start at the 150 data samples.....	19
Figure 4.1. Proposed Single Capacitor Dual Receiver WPT Circuit	21
Figure 4.2. Common Dual Receivers WPT Circuit with Capacitor Compensation in Each Receiver. .	23
Figure 4.3. Preliminary Computation Results of f_1 and f_2 with Numerical Values in 0 where $K_1 = K_2$ and $K_3=0$	25
Figure 4.4. Preliminary Computation Results of f_1 and f_2 with Numerical Values in Table 4.1 where K_1 is free variables, $K_2 = 0.3$ and $K_3=0$	26
Figure 4.5. Optimization Results for objective functions in equation (27) Using Numerical Values in 0 where $K_{12} = K_1=K_2$ and $K_3=0$	28
Figure 4.6. LTSPICE Results Plotted using Python for obtained design values in Table 4.2.	29
Figure 4.7. LTSPICE Results Plotted using Python for obtained design values in 0	30
Figure 4.8. Optimization Results for objective functions in equation (29) Using Numerical Values in Table 4.4.....	31
Figure 4.9. LTSPICE Results Plotted using Python for obtained design values in Table 4.5.	32
Figure 4.10. Power at RL_1 and RL_2 using proposed circuit and optimization method with $C=21.4$ nF and $freq=243.89$ kHz (Obtained from LTSPICE simulations).....	34
Figure 4.11. Power at RL_1 and RL_2 in Fig.2. circuit and idea of resonance calculation using $C_1 = C_2 = C_3 = 110$ nF. (Obtained from LTSPICE simulations)	34
Figure 4.12 Running Metrics Analysis	36

List of Tables

Table 2.1. Parameters Value.....	8
Table 3.1. Set of peak candidates, error computation, optimal frequency decision, and validation. Obtained during 159 data with ten peaks found by the AMPD Algorithm.	16
Table 3.2. The set of peaks (l) comparison between the spotting method result and correct (l) set of peaks obtained from direct observation.....	17
Table 3.3. Error distance comparison between the spotting strategies set of peaks with 159 samples with the direct observation with 950 data.....	18
Table 4.1. Numerical Component value	25
Table 4.2. Figure 4.5 Decision Making Results.....	28
Table 4.3. Decision Making Results.....	30
Table 4.4. Component values for optimization with capacitance and frequency as design variables	31
Table 4.5. Figure 4.8 Decision Making Results.....	32
Table 4.6. Component values for scenario 1.....	33
Table 4.7. Design Spaces Comparison Result.....	35
Table 4.8. Optimization Time	37

Chapter 1

Introduction

1.1 Background

Wireless Power Transfer (WPT) can supply electric power to an electric device without wires. Began in 1889, the innovation of the Tesla coil by Nicola Tesla realizes the idea of WPT when a light bulb is lit from some distance [1]. Tesla recognition has made the inductive WPT one of the researcher's common methods to deliver power wirelessly. This idea wants to be implemented by electronic appliance companies to avoid complex wire connections. Hence, the increasing WPT demand for electronic handheld and compact devices (mobile phone, laptop, tablet, Etc.). Until present, the WPT technology to supply compact electronic devices at close gap have been reaching standardization and available as a consumer product [2].

The inductive WPT research is accelerating further to improve the gap distance and power delivery [3] [4] [5] [6]. The basic inductive WPT circuit can be implemented using pair of coils in the primary and secondary circuit, which works as self-inductance and is affected by its mutual inductance [7]. This minimum WPT circuit can only deliver a small amount of power compared to the wired connection. Therefore, to increase the amount of power absorbed by the load, the circuit needs an additional inductor or capacitor in the primary, secondary, or both circuits. This method is known as the compensation technique [8] [9]. The most common method for compensating the inductive WPT circuit is using capacitance components in the primary and secondary sides to form a symmetric WPT circuit [10]. Then, the high-power delivery is obtained through resonance, which is a phenomenon that occurs in the circuit with the AC voltage source. The resonance phenomenon occurs when the coils' inductive reactance equals the capacitive reactance of the capacitor at some frequency points (resonant frequency). However, the violation and incapability of the idea of resonance may occur in practical situations. This situation happens when the WPT system becomes asymmetrical (non-resonant situation) or in the asymmetric WPT circuits.

The violation of resonance frequency to deliver high power can occur because of coils misalignment, gap change, or indeterministic secondary receiver [11] [12] [13]. In this condition, a resonant frequency calculation to obtain operating frequency cannot be used, and system model computation should be conducted to obtain the behavior from a WPT system. High power can be obtained through the model and frequency response analysis by knowing all parameters value other than frequency. Although the problem can be answered theoretically, another practical challenge occurs caused by a coupling coefficient parameter that represents the coils misalignment and gap. This coupling coefficient described as a value between 0-1, with both coils is having the same winding direction. Therefore, even though the high power

can be obtained using the system models and frequency response analysis, understanding the practical situation of how much coupling coefficient representing the gap/misalignment is challenging [14] [15]. In this meaning, the inverse problem of finding high-power operating frequency is an open challenge in the WPT research field. Tracking the operating frequency without considering the number of frequency sweep is a time-consuming process. Therefore, by considering the number of frequency sweeps, a method improvement for tracking and validating optimal frequency needs to be conducted.

Since the resonant frequency calculation is violated in some conditions, the usage of capacitance at the secondary receiver becomes questionable. Adding components to compensate WPT circuit (ex: adding a capacitor in each receiver) can increase the circuit's equivalent series resistance so that it can affect the power and efficiency of the WPT system [16] [17] [18]. Furthermore, the capacitor addition on the multi-receivers WPT becomes more complex along with the number of receivers. For this reason, a question regarding the ability to obtain high power on a single capacitance asymmetric WPT circuit needs to be addressed.

This study presents an approach to obtain the high power from an asymmetric situation that cannot use the idea of resonance. A fast-spotting strategy to find optimal frequency has been proposed to obtain high-power WPT in practical situations by considering the numbers of the frequency sweep. Next, this study also presents an approach to obtain high-power delivery on asymmetric WPT circuits by highlighting the simplicity of capacitance-less multi-receivers.

1.2 Research Objectives

The objectives of this study are:

1. Study the common symmetric WPT circuit to deliver a high power, using the idea of resonance. Investigate the resonance calculation results with the system behavior obtained from a frequency response through a model.
2. Provide a solution to obtain operating frequency to deliver high power to the secondary circuit without the idea of resonance. The solutions provided should consider the number of frequencies sweeping to avoid a time-consuming sweeping process.
3. Propose an approach to achieve wireless high-power transfer on the asymmetric circuit that highlights capacitance-less receiver circuit.

1.3 Research Scope

The near-field WPT with almost zero gaps has been established, standardized, and commercialized (Qi [2]). Therefore, the current research of WPT advances in improving the gap size and power delivery. The most common method to deliver high power in the WPT system is by utilizing pairs of inductance and capacitance on both primary and secondary sides to form an ideal symmetrical condition. In the practical challenge, the condition might become asymmetry when the WPT circuit has undetermined parameters value or when the WPT circuit only compensates by primary side capacitance. Therefore, this study investigates the resonant situation and the behavior of the symmetric WPT circuit theoretically. Then, this

study describes an alternative approach to achieve high power without the idea of resonance. This study also contributes to a method to obtain high power in the asymmetric circuit where the idea of resonance cannot be implemented. The scope of this study is presented in Figure 1.1.

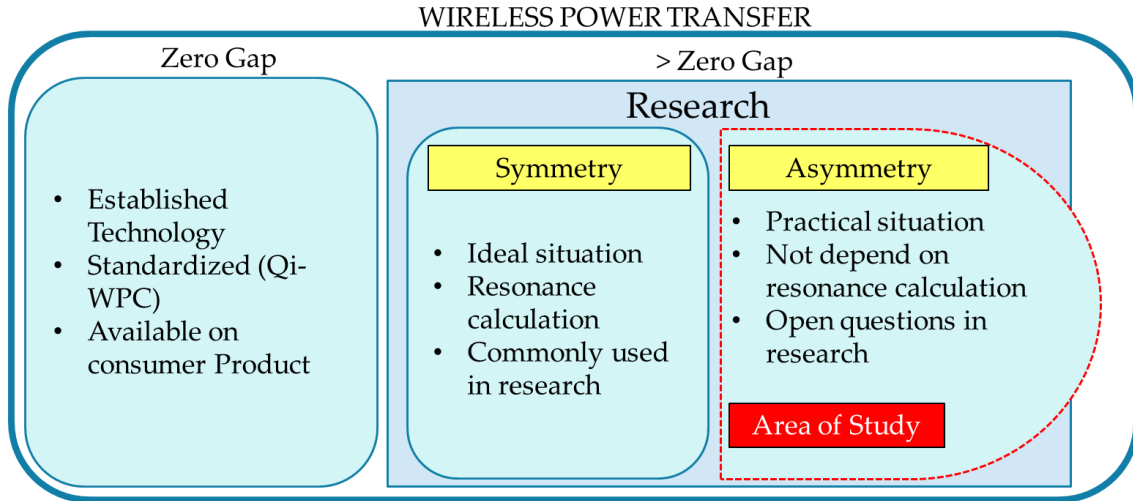


Figure 1.1. Research Scope

1.4 Contributions and Findings

This study contributes to the study of resonant condition on the symmetric circuit by analyzing the circuit behavior through system model of symmetric WPT circuit. Afterwards, the investigation of the non-resonant and asymmetric circuits has been presented through two main findings which are:

1. An approach to obtain global peak of power on the WPT system that avoid time-consuming frequency sweep using stimulated response by the square wave input signals.
2. An approach to obtain high power using optimization on an asymmetric WPT circuit even by eliminate the receiver circuit capacitance.

1.5 Outline

This dissertation consists of 5 chapters:

Chapter 1 introduction. This chapter explains the background regarding the current situation of WPT research and the explanation of resonant (symmetry) and non-resonant (asymmetry) situations. This chapter also presents the objective of the study, followed by the scope, contributions, and findings.

Chapter 2 Resonance and Symmetric Circuit. This chapter is explaining the common symmetric WPT circuit and the idea of resonance. This study observed the behavior of the symmetric WPT system by obtaining the circuit model through transfer function calculation.

Afterwards, the situation of the WPT system presented in the form of frequency response and transient analysis.

Chapter 3 A Fast-Spotting Strategy of Optimal Frequency in Wireless Power Transfer. This chapter is presenting a method to obtain the high-power delivery without using the idea of resonance using a fast frequency spotting strategy using a square wave input power signal.

Chapter 4 A Design Approach to Wireless High-Power Transfer to Multiple Receivers with Asymmetric Circuit. This chapter is presenting methods to obtain high-power in the asymmetric circuit, a circuit whether the idea of resonance is cannot be used. This section presenting an optimization approach to obtain the optimal parameters in several design challenges.

Chapter 5 Summary This chapter gives a summarization of studies and conclude the results regarding the investigation of idea of resonance and symmetric circuit, and the approaches to obtain high-power without the idea of resonance or in an asymmetric circuit. Moreover, this chapter explain the future works based on the current study.

Chapter 2

Resonance and Symmetric Circuit

Generally, the investigation and analysis of the WPT system want to obtain the absorbed power by the load or system efficiency. Moreover, it is important to analyze the stimulus-response of the system and the transient steady-state analysis to understand the system's behavior in the frequency and time domain. Therefore, this study discusses the theorem of WPT in the scope of the process regarding how we obtain the WPT model and investigate the system behavior. The process is shown in Figure 2.1 and describes more details in the sub-chapter.

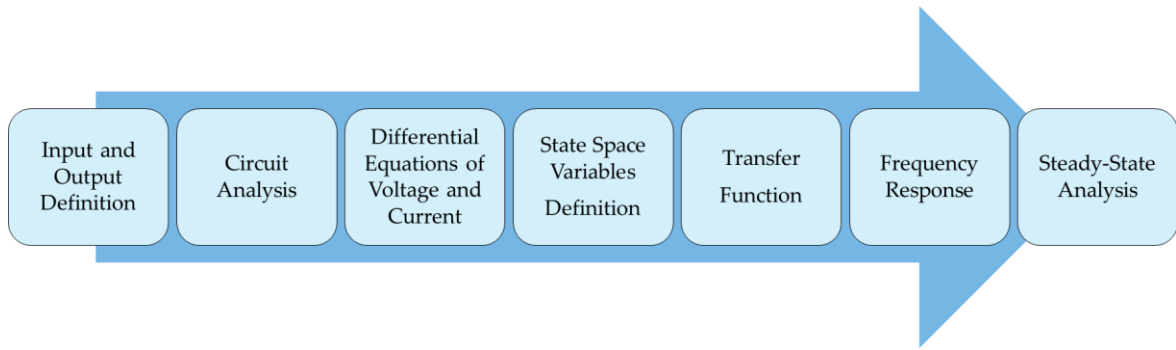


Figure 2.1. Wireless Power Transfer

2.1 Wireless Power Transfer Symmetric Circuit

WPT's objective is to deliver power originating at the primary side's power source to load R_L on the secondary side. The basic circuit of inductive WPT is consists of the primary side coil (L_1) and secondary coil (L_2). Then, it is common to add capacitors on both sides (C_1 and C_2) to use the idea of resonance. The resonance phenomenon occurs in a circuit with the AC voltage source where the coils' inductive reactance equals the capacitive reactance of the capacitor at some frequency points (resonant frequency). Therefore, a common WPT circuit is configured using a symmetry LC series on both sides to obtain high power delivery, as shown in Figure 2.2. Then, the resonant frequency points can be calculated using the resonant formula (1).

$$f = \frac{1}{2\pi\sqrt{L_1C_1}} = \frac{1}{2\pi\sqrt{L_2C_2}} \quad (1)$$

The Figure 2.2 primary circuit consists of an input voltage source (u) with an internal resistance R_S , a capacitor (C_1), the coil inductor (L_1), and its coil resistance (R_1). The secondary circuit consists of the receiver coil (L_2), a capacitor (C_2), its resistance (R_2), and the load (R_L). M is the mutual inductance between the coils can be described as coupling co-efficient (K) can

be replaced with (2). The coupling coefficient K is a coefficient between 0-1 (Assuming the same direction of winding between coils) that can be represented as the gap between coils or misalignment [19].

$$K = \frac{M}{\sqrt{L_1 L_2}} \quad (2)$$

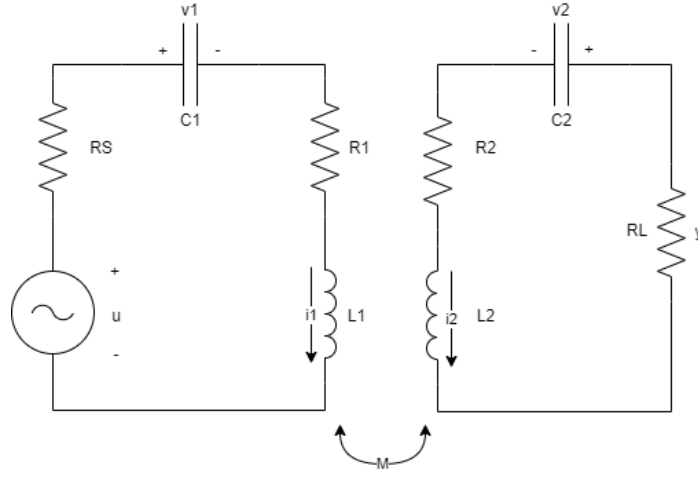


Figure 2.2. Wireless Power Transfer Symmetric Circuit

This study is interested in the high-power delivery absorbed by R_L , then the input voltage (u) and the output voltage R_L (y) are defined as the input and output of the system. The current flows in the primary and secondary coils are described as i_1 and i_2 . v_1 and v_2 describe the voltage of capacitor at the primary and secondary circuits. Then, by using Kirchhoff's Current and Voltage Law, we can obtain the differential equations of the circuit as (3).

$$\begin{aligned} \frac{dv_1}{dt} &= \frac{i_1}{C_1} \\ \frac{dv_2}{dt} &= \frac{i_2}{C_2} \\ \frac{di_1}{dt} &= \frac{-L_2(R_1 i_1 + R_S i_1 - u + v_1) + M(R_2 i_2 + R_L i_2 + v_2)}{L_1 L_2 - M^2} \\ \frac{di_2}{dt} &= \frac{-L_1(R_2 i_2 + R_L i_2 + v_2) + M(R_1 i_1 + R_S i_1 - u + v_1)}{L_1 L_2 - M^2} \end{aligned} \quad (3)$$

2.2 System Model of Wireless Power Transfer

The WPT transfer function as a system model can be obtained through the state space equation [20] [21]. The state-space equation is used to describe the algebraic model of the system as we expressed the input voltage (u) and the output voltage R_L (y) in a transfer function by using v_1 , v_2 , i_1 , and i_2 as the state space variables. from general state space representation in (4), by selecting v_1 , v_2 , i_1 , i_2 as our state space variables, we define our state space representations as (5).

$$\begin{aligned} \dot{x} &= Ax + Bu \\ y &= Cx + Du \end{aligned} \quad (4)$$

$$\begin{bmatrix} \frac{dv_1}{dt} \\ \frac{dv_2}{dt} \\ \frac{di_1}{dt} \\ \frac{di_2}{dt} \end{bmatrix} = A \begin{bmatrix} v_1 \\ v_2 \\ i_1 \\ i_2 \end{bmatrix} + Bu \quad (5)$$

$$y = C \begin{bmatrix} v_1 \\ v_2 \\ i_1 \\ i_2 \end{bmatrix} + Du$$

Then, from (3) and (5), matrix A, B, C, D can be described as (6).

$$A = \begin{bmatrix} 0 & 0 & \frac{1}{C_1} & 0 \\ 0 & 0 & 0 & \frac{1}{C_2} \\ -\frac{L_2}{L_1L_2 - M^2} & \frac{M}{L_1L_2 - M^2} & \frac{-L_2R_1 - L_2R_S}{L_1L_2 - M^2} & \frac{MR_2 + MR_L}{L_1L_2 - M^2} \\ -\frac{M}{-L_1L_2 + M^2} & \frac{L_1}{-L_1L_2 + M^2} & \frac{-MR_1 - MR_S}{-L_1L_2 + M^2} & \frac{L_1R_2 + L_1R_L}{-L_1L_2 + M^2} \end{bmatrix} \quad B = \begin{bmatrix} 0 \\ 0 \\ \frac{L_2}{L_1L_2 - M^2} \\ \frac{M}{-L_1L_2 + M^2} \end{bmatrix} \quad (6)$$

$$C = [0 \quad 0 \quad 0 \quad -R_L]$$

The transfer function (8) from u to y is given by (7)

$$\frac{Y(s)}{U(s)} = C[sI - A]^{-1}B \quad (7)$$

$$= \frac{C_1C_2MR_Ls^3}{C_1C_2s^2\Delta + s^2(C_1L_1 + C_2L_2) + s(C_1R_1 + C_1R_S + C_2R_2 + C_2R_L) + 1} \quad (8)$$

Where,

$$\Delta = (R_1R_2 + R_1R_L + R_2R_S + R_LR_S + s^2(L_1L_2 - M^2) + s(L_1R_2 + L_1R_L + L_2R_1 + L_2R_S))$$

2.3 Frequency Response

In the symmetric circuit Figure 2.2, the idea to obtain high-power delivery is by finding the resonant frequency. Therefore, using inductance and capacitance parameters in Table 2.1, we can calculate the resonant frequency is at 54.05 kHz on the primary circuit and 54.92 kHz on the secondary circuit. The resonance calculation is interesting since there is a slight difference on both sides of the frequency resonant. Hence, obtain the resonant frequency is only able to be accomplished in the ideal situation.

Table 2.1. Parameters Value

$L_1=900\mu H$	$L_2=82.4\mu H$	$C_1=9.6nF$	$C_2=100nF$
$R_S=0.1\Omega$	$R_1=0.44\Omega$	$R_2=0.17\Omega$	$R_L=20\Omega$

After the system model is obtained through transfer function calculation (8), the frequency response analysis able to be conducted after (8) transformed into the frequency domain. Then, using the value of the parameter in Table 2.1 and (8). With a small AC signal $u_0 = 1 V$, the frequency is swept at a 100-100 kHz range. The plot of the frequency response with respect to R_L power is shown in Figure 2.3 using input square wave and sine wave. From the results, we obtain the optimal frequency at 54 kHz. The square wave frequency response shows whether several peaks exist at the swept frequency. The square wave input has a Fourier coefficient pattern consisting of a global peak frequency, 1/3 global peak frequency, 1/5 global peak frequency, Etc. These peaks can be selected when the WPT system design has some specific frequency constrain. Moreover, this information is helpful for global peak searching since it can validate the global peak frequency position.

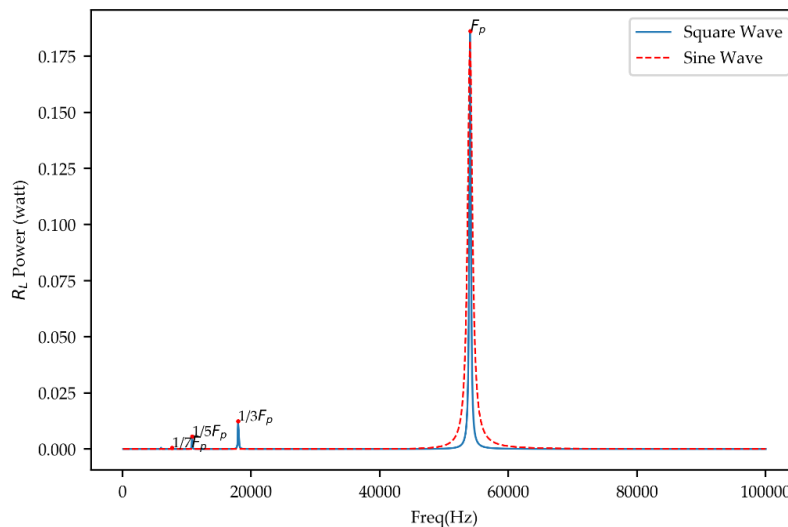


Figure 2.3. Frequency Response using Square Wave and Sine Wave

2.4 Steady-State Analysis

Our circuit equation stimulated by a periodic input has a periodic solution with the period same as the input, since the differential equation is a linear time-invariant system. If the system is stable, i.e., all the eigenvalues of the matrix A have a negative real part, then the periodic solution will be asymptotically stable. In other words, any solution starting with any initial value will behave like the periodic solution when the time has passed enough; thus, the periodic solution is often called a steady-state solution [22]. In the beginning, it is important to obtain the steady-state function to get the exact calculation in the steady-state conditions [23] [24]. Since this study analyzes the circuit's behavior using the sine wave input, the input function $u(t)$ can be described as (9), where u_0 is the amplitude of the input voltage.

$$u(t) = u_0 \sin(\omega t) \quad (9)$$

From the sinusoidal input (9) the steady-state function of the y_{ss} can be described as in (10) [25].

$$y_{ss}(t) = u_0 |G(j\omega)| \sin(\omega t + \angle G(j\omega)) \quad (10)$$

The $p_{ss}(t)$ is power at the load R_L in steady state. The average of $p_{ss}(t)$ over a period is called an average power at the load R_L can be obtained using (11). Then, using the parameters value in Table 2.1, $K=0.3$ and frequency 53.41 kHz the steady-state plot of voltage and power in R_L are plotted in Figure 2.4.

$$p_{ss}(t) = \frac{y_{ss}^2(t)}{R_L} \quad (11)$$

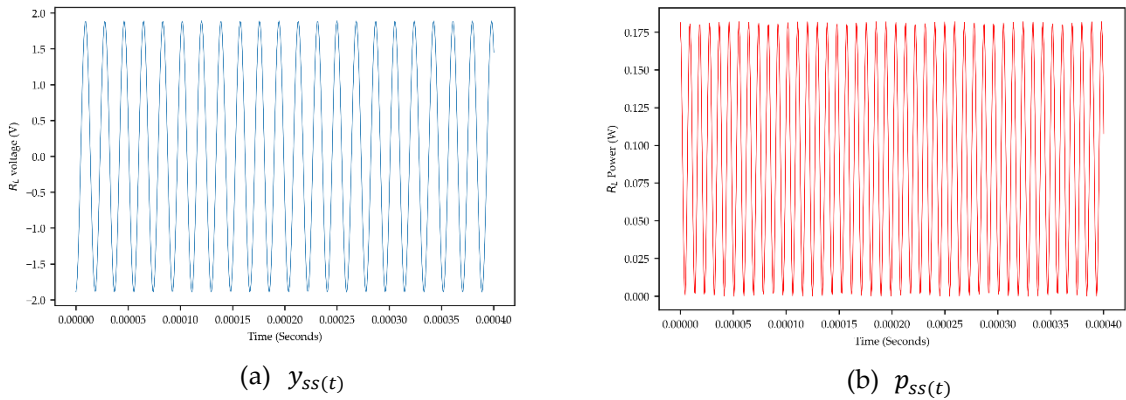


Figure 2.4. the steady-state plot of voltage ($y_{ss}(t)$) and power ($p_{ss}(t)$) in R_L

2.5 Optimization of Power

Using Table 2.1 and (11) we able to obtain the R_L power frequency response as in Figure 2.5. Using small AC signal $u_0 = 1 V$ and the frequency is swept between 100 Hz-100 kHz, the R_L power frequency response is shown in Figure 2.5. By giving various value of K this study obtain that the resonant frequency is not always obtaining the highest power since the optimal frequency are changed on different coupling coefficient (K) situation.

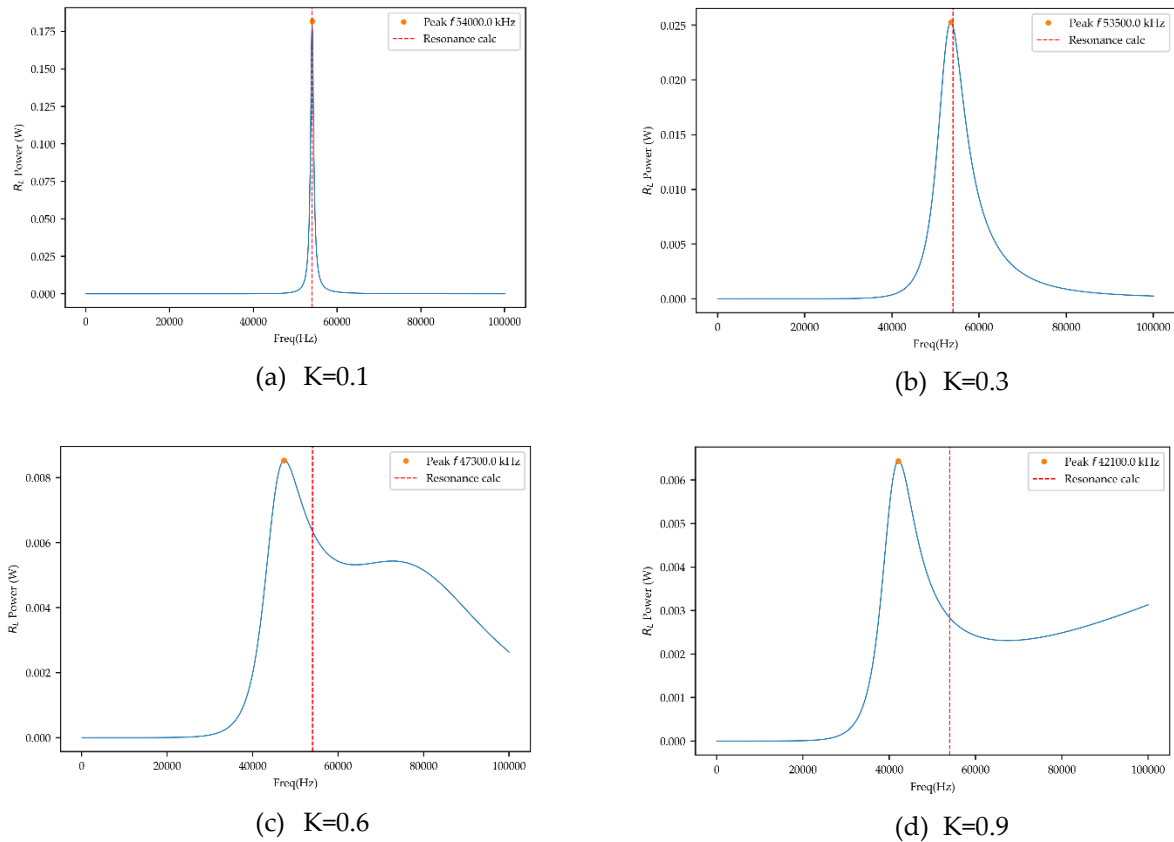
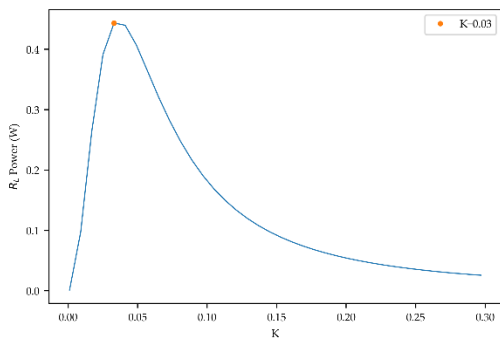
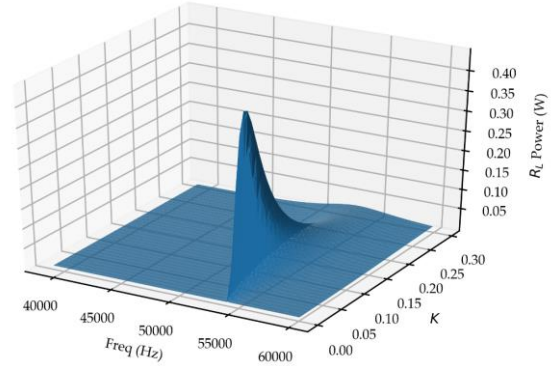


Figure 2.5. R_L Power Frequency Response of Symmetric WPT Circuit

More investigation is conducted to understand the optimal K position by giving smaller range of K coupling coefficient. Afterwards, for each of K coupling coefficient, the frequency is swept between 100 Hz-100 kHz and the global peak is obtained for each K . The result is obtained as in the Figure 2.6. We obtain whether the value of K is at 0.03 position and will be decreased when the value of K is getting smaller.



(a) Optimal K



(b) 3D Representation of Optimal Power

Figure 2.6. Optimal Power

In this meaning, the optimal absorbed power at R_L can be reached when the frequency and K coupling coefficient is optimized at some points. Other than K coupling coefficient, the frequency of the WPT system is affected by the value of inductance and capacitance (obtained from model). Therefore, in the next chapter, this study shows the investigation on the WPT system optimization by considering the combination of 3 design variables (capacitance, frequency, K coupling coefficient and inductance, capacitance, K coupling coefficient).

Chapter 3

A Fast-Spotting Strategy of Optimal Frequency in Wireless Power Transfer

3.1 Background

WPT is one of the promising technologies to provide a sustainable future since it could reduce the usage of batteries and cables on electronic appliances [26]. Started by the Tesla experiment [1], the WPT methods had classified into a radiative category (such as using a microwave) and non-radiative category that uses the inductive and capacitive power transfer [27]. The inductive power transfer method has gained popularity stimulated by the research [28] in 2007, where non-radiative inductive power transfer successfully transferred 60 watts within 2 meters range and get 40% of efficiency. Currently, the WPT has been implemented in many applications such as electric vehicles [29], consumer appliance [30], Internet of Things [31], and biomedical applications [32].

Improvement of power transfer efficiency to deliver much power over coils is a challenge in WPT. Several methods to improve efficiency have been review in [23], including impedance matching [33], parameter optimization [21], and selection of an optimal frequency [34]. Furthermore, to reach the required efficiency, several efficiency-tracking methods have been proposed, such as dynamic coupling coefficient estimation [35], phase shift [36], and adaptive frequency [37]. Therefore, the WPT overall system performance depends on several key parameters such as frequency, the shape of input power source signal, type and section of coils, the radius of coils, and transfer distance [3].

The power transfer efficiency requested can be found by knowing and giving a fixed parameter value. However, once the parameter changes, the efficiency of power transfer will decrease since the optimum parameters were only suitable for the previous condition. Optimum power transfer for the current situation was only able to be obtained by parameter recalculation and re-finding. In this meaning, the inverse problem of finding optimum parameters for a continuously changing situation is an open challenge in the WPT research field. Impedance and resonant frequency parameters (In the case of frequency) towards the coil distance variation is a situational example that can reduce the efficiency of a WPT system [37]. This problem can be avoided by always giving the correct frequency input to the WPT system by using frequency tracking and tuning. Frequency tracking and adjustment have been demonstrated in some research [37] [38] [34] [39]. However, tracking the optimal frequency without considering the number of frequency sweep is a time-consuming process. Therefore, by considering the number of frequency sweeping, a method improvement for tracking and validating optimal frequency needs to be conducted.

This paper concerns how to determine the frequency of AC power source optimal to maximum WPT. An optimal frequency can be found accurately by applying frequency sweep. However, the frequency sweeping takes a long time, and there is a high possibility that the parameters and situations might change during the process. This paper proposes a strategy to find and validate the optimal power transfer frequency in WPT with a square wave input signal. Compared to the sine wave, the square wave input signals can deliver higher power even if the input frequency restricted to a lower frequency than the resonant frequency [6] [40]. Furthermore, by using Fourier analysis of the response stimulated by the square wave input signals, the optimal power transfer can be validated, since the optimal frequency has a set of peak patterns between the frequency ranges.

3.2 Proposed Method

In the preliminary research and experiment, the WPT system received a 5-100 kHz (with a 100 Hz interval) square wave input signal. We obtained 950 power data from the receiver with a 20-Ohm load resistance and 35mm distance between coils. Thus, based on the experiment result observation, a set of essential peaks (l) was found, including the optimum frequency that delivers the highest power to the receiver. Figure 3.1 shows obtained data include the optimal power transfer frequency 56.9 kHz (l_0), followed by other local peaks $\{l_1, l_2, l_3, l_4\}$, located 18.2 kHz, 11 kHz, 7.8 kHz, and 5.9 kHz, respectively.

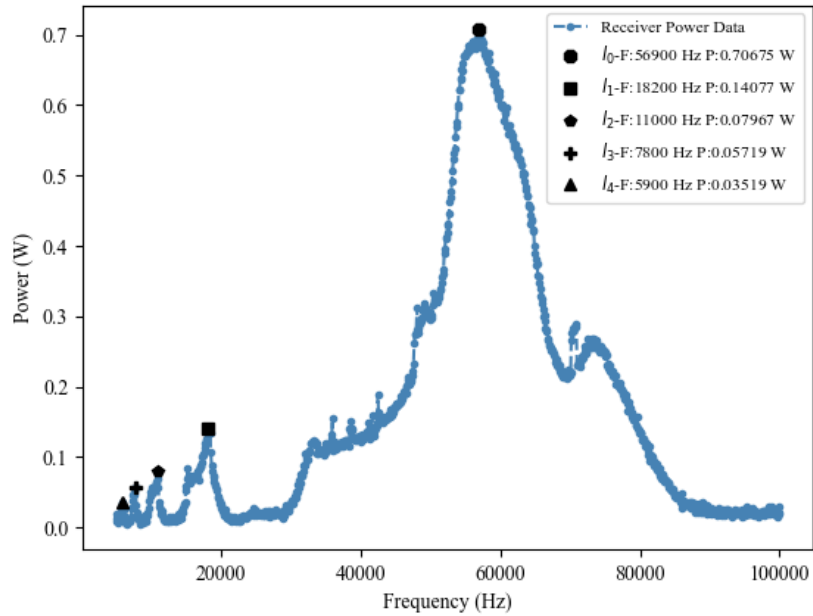


Figure 3.1. Transferred power to 20 Ohm load depending on the driving frequency (experiment).

Furthermore, let $l = \{l_0, l_1, l_2, l_3, \dots, l_n\}$, with respect to frequency, the pattern formula from a set of peaks was obtained and shown in the equation (12). Moreover, since the square wave signal has 3rd, 5th, 7th, nth-times frequencies in addition to the fundamental frequency,

deciding an optimal frequency will be possible, by referring this knowledge to discover the set of peak patterns.

$$l = \left\{ l_0, \frac{1}{3} l_0, \frac{1}{5} l_0, \frac{1}{7} l_0, \frac{1}{9} l_0, \dots, \frac{1}{2n+1} l_0 \right\} \quad (12)$$

Our spotting method uses the AMPD algorithm [41] to find the initial peak since it is suitable for our WPT system that has a set of peak patterns with a multiscale periodic type of peaks [42] [43]. The AMPD algorithm will collect the initial peaks to further analyze by our spotting method. Afterward, our spotting method will determine the optimal frequency by validating its existence on each set of sample data. If the spotting method recognized the set of peaks, the optimum power transfer value could be obtained. The generic process from the proposed method illustrates using the flowchart shown in Figure 3.2.

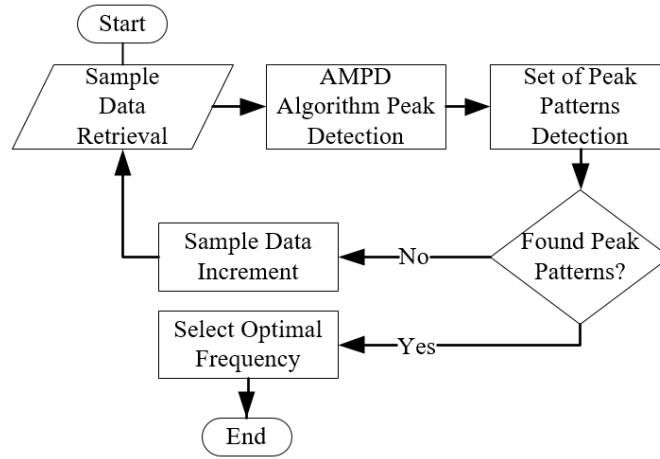


Figure 3.2. Proposed Method Flowchart

By using the (12) as a rule to validate the optimal frequency, the proposed spotting method is described as follows:

1. Retrieve a sample of data in 5-100 kHz starting from 10 kHz sampling interval (i). Collect a set of peaks by using the AMPD algorithm (p) in sample data by using several intervals.
2. Increase the length of sample data until the length of p is higher or equal to the length of peak pattern to be found (n).
3. Afterward, the optimal frequency (l_0) assumption (g) is decided by finding the highest power in p . The next $l_1, l_2, l_3, \dots, l_n$ pattern approximation are found by computing a set of peak approximation frequency (a) by multiplying g with $\frac{1}{2n+1}$.
4. For each a , find the nearest frequency as a candidate peak (c) for each in p and measure the distance error (e_d) by averaging $\frac{|c_n - a_n|}{95000}$, where 95000 is the observed frequency width (5-100 kHz).
5. Measure the amplitude error by identifying whether the amplitude for each $c_n > c_{n+1}$ is satisfied using Boolean value, or not. If the result is false, then $e_a = 1$ otherwise $e_a = 0$.

6. Decide the optimal frequency validity by computing total error $e_{total} = (0.2e_d + 0.8e_a)$, where 0.8 weight given to e_a since a e_a error is unacceptable. Therefore, if the result of e_{total} is higher than 0.8, the status of the optimal frequency will be considered invalid, and more data samplings are required.
7. Check whether all l_n has been find and e_{total} is less than 0.8. Increase the sample data if some l_n is missing or less then the n requested.

Increment of the sample data will include the previously gathered data appended with new sample data. The new sample data obtained by reducing the starting frequency interval (i) by a decrement variable (d) that decided by the experiment shown in Figure 3.3 The iteration process will continue until $i = 0$.

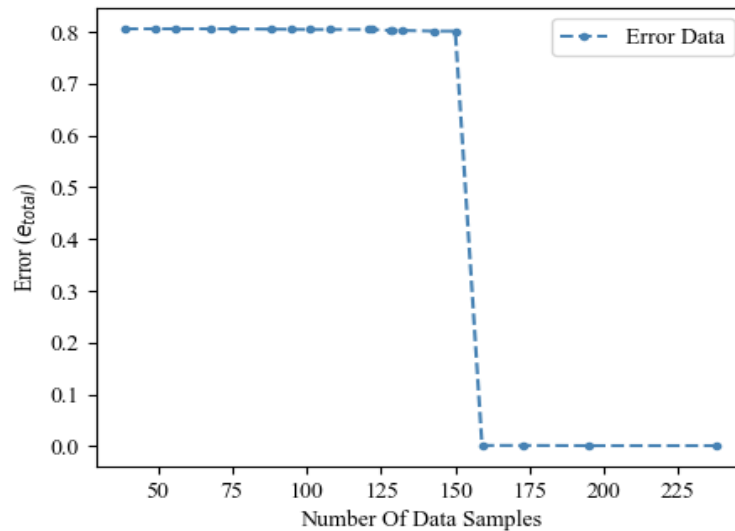


Figure 3.3. The experiment conducted to collect e_{total} on each iteration with $d=400$. The data sample increment (i) starts with 10 kHz interval and find the e_{total} value from 5-100 kHz.

3.3 Result and discussion

The spotting strategies implemented using Python programming language and the experiment begin by finding the decrement interval variable. The experiment conducted by collect e_{total} on each iteration, as shown in Figure 3.3. In the first iteration, ten data samples obtained with a 10 kHz interval. Since the e_{total} is higher than 0.2, the optimal frequency considered to be invalid, and it will continue to the next iteration. Sample data will be propagated (include the previously retrieved data) by subtracting the current i by 400. Therefore, on the next iteration, sample data will be appended every 9.6 kHz.

The iteration will continue until $i = 0$, and in this experiment, 238 sample data were able to be collected. Based on Figure 3.3 observation, the optimal frequency can be determined since the number of samples of data reaches 159 samples. Therefore, by capturing e_{total} on each iteration, the optimal frequency was able to be decided whenever the e_{total} value is less than 0.8 in some iterations. Figure 3.4 shows the situation when the AMPD algorithm finds the

peaks based on 159 data samples. The AMPD algorithm collected ten peaks for further analyze by the spotting method to find the correct set of peaks.

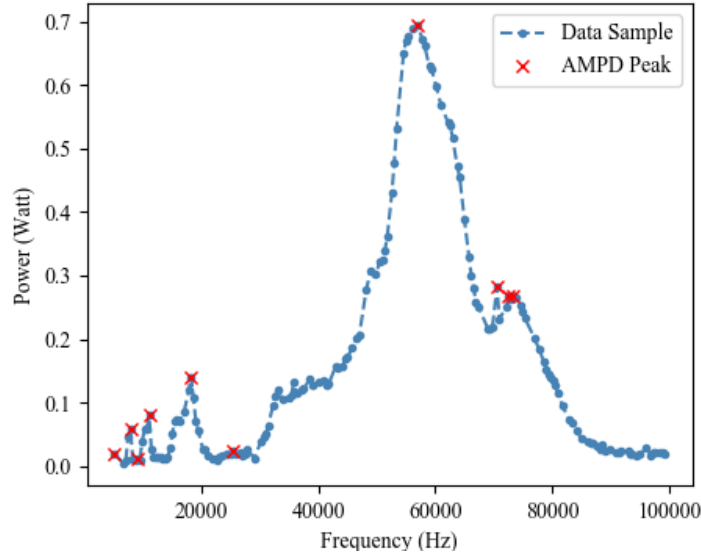


Figure 3.4. The Experiment during the 159 data samples with 10 peaks found by the AMPD Algorithm.

Table 3.1 shows the result when the iteration reaches a total of 159 data samples. The e_a shows a small 0.005464 value, which means the approximation value (a) for each local peak is found in the peak collect by the AMPD Algorithm. The e_a is 0 since the condition of the power amplitude for $c_0 > c_1 > c_2 > c_3 > c_4$ was true. Afterward, the e_{total} will be calculated and use to select a set of peaks $l = l_4, l_3, l_2, l_1, l_0$, as shown in Figure 3.5.

Table 3.1. Set of peak candidates, error computation, optimal frequency decision, and validation. Obtained during 159 data with ten peaks found by the AMPD Algorithm.

Highest Power Frequency Found by AMPD algorithm (p)		Set of Peak Candidate (c) (Hz)				Error		
Frequency (c_0) (Hz)	Power (Watt)	c_1	c_2	c_3	c_4	e_a	e_a	e_{total}
57000 (l_0)	0.694	18200 (l_1)	11000 (l_2)	7800 (l_3)	5000 (l_4)	0.005	0	0.001

To validate the result obtained by the AMPD and the spotting method, we compare the set of peak l results from Figure 3.5 with the real peak obtained from direct observation, as shown in Table 3.2. This result showed that the optimal power transfer frequency obtained from the proposed algorithm has a 0.17% error distance from the real optimum. Furthermore, this algorithm can continue to retrieve the data among the peak width if a more accurate result is required.

Table 3.2. The set of peaks (l) comparison between the spotting method result and correct (l) set of peaks obtained from direct observation.

Set of peak patterns (l)	Peak detection with 205 data (Hz)	Power (Watt)	Peak Width Range (Hz)	Real peak Frequency (Hz)	Power (Watt)	Error Distance (%)
l_0	57000	0.694	51800-65800	56900	0.706	0.175
l_1	18200	0.008	16200-19000	18200	0.147	0
l_2	11000	0.079	9800-11400	11000	0.079	0
l_3	7800	0.057	7400-8200	7800	0.057	0
l_4	5000	0.019	5000-5000	5900	0.035	15.254

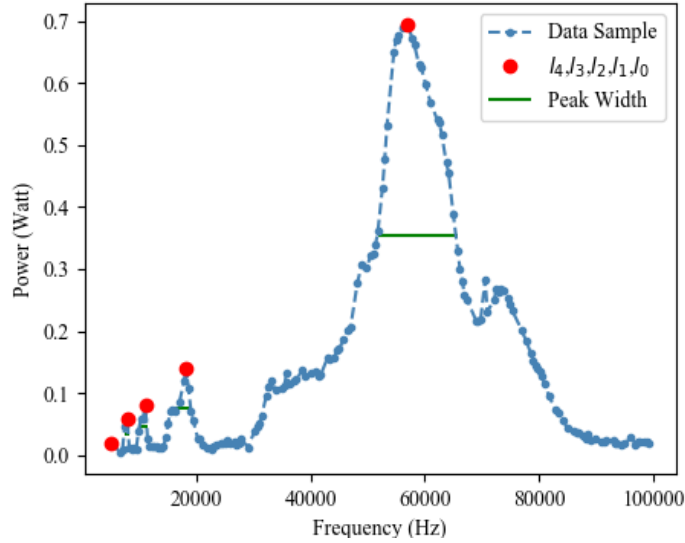


Figure 3.5. The 159 data samples with set of peaks ($l = l_4, l_3, l_2, l_1, l_0$) respectively from smallest to highest frequency alongside with the peak width, after being selected by the spotting strategies

The second experiment conducted to evaluate the spotting method works well in different experimental data. Figure 3.6 shows additional data that have similar characteristics. These three data have a different optimal frequency, although the location of the peaks is close to each other. The same scenario was conducted, which is to check the e_{total} plot on each iteration with the starting frequency (i) is 10 kHz, and the decrement variable (d) is 400 Hz. Afterward, we check the plot result and find the first condition where $e_{total} < 0.8$ on both data. In the last step, we compare the result with the peak obtained from the direct observation.

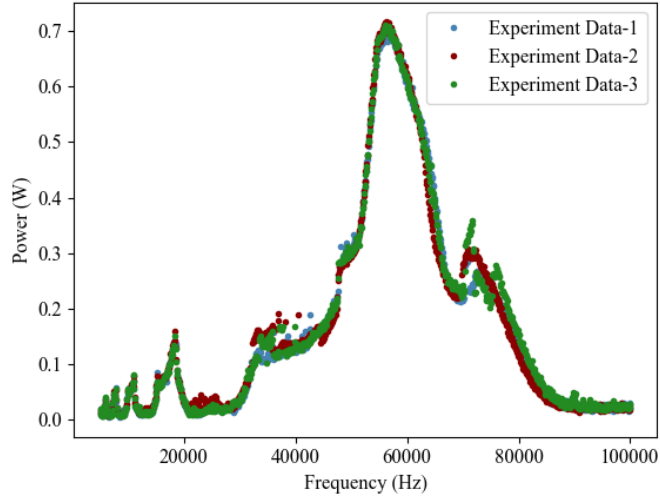


Figure 3.6. Three experimental data consists of 950 power data, received from WPT system by 20 Ohm resistor using square wave input signal.

Figure 3.3 shows the e_{total} plot for data-1. While Figure 3.7 and Figure 3.8 display the e_{total} plot for data-2, and data-3, respectively. Both figures show that the optimal frequency discovers when the spotting method detects $e_{total} < 0.8$ condition. The optimal frequency validated after the iteration reach 173 data samples on the data-2 and 150 data samples on the data-3. Thus, the proposed spotting method is successful in finding the optimal frequency without a time-consuming sweeping process.

Table 3.3. Error distance comparison between the spotting strategies set of peaks with 159 samples with the direct observation with 950 data.

Data	AMPD Peak Find	Total Data	The spotting strategies error distance (%) compared to the real distance by direct observation					Optimal Power Difference (Watt)
			l_0	l_1	l_2	l_3	l_4	
1	10	159	0.175	0	0	0	15.254	0.012
2	18	173	0	1.086	0	0	16.667	0
3	5	150	0.178	1.086	0	0	16.667	0.006

Table 3.3 shows the error distance of the set of peaks found by the spotting method compared with the direct observation. The result shows that the accuracy of the proposed spotting method to find an optimal frequency (l_0) achieves a minimal error, and a small difference in the power received. However, l_4 distance error accuracy is high since the peak shape in the l_4 has short prominence proved with the peak width analysis in Table 3.2. A frequency sweeping can be performed among the peak width on the discovered l_0 frequency to increase the accuracy to find the optimal frequency. Nevertheless, this process depends on the requirement, since on this experiment, the received power difference is small.

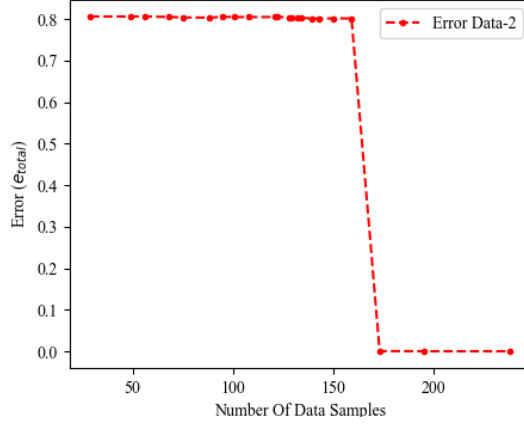


Figure 3.7. The experiment conducted to collect e_{total} on each iteration with $d = 400$ from a total 238 of data samples in Data-2 with the $e_{total} < 0.8$ start at the 173 data samples.

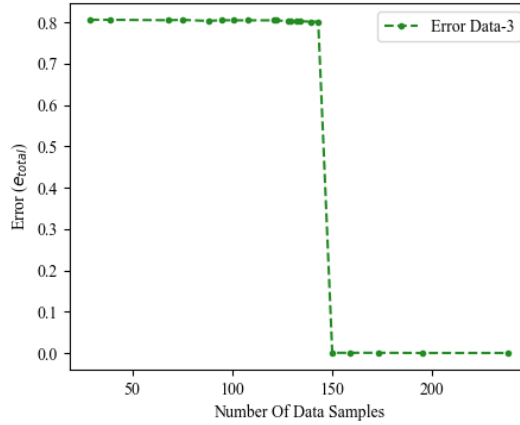


Figure 3.8. The experiment conducted to collect e_{total} on each iteration with $d = 400$ from a total 238 of data samples in Data-3 with the $e_{total} < 0.8$ start at the 150 data samples.

3.4 Conclusions

Finding optimal driving frequency as fast and accurate as possible is essential in any WPT system to transfer much power over coils driven by the AC power source. This paper has proposed a spotting strategy to find the optimal frequency by using Fourier analysis of the response stimulated by the square wave input signals. The spotting method avoids a time-consuming sweeping process by using initial peak selections from the AMPD algorithm. From the experiment, our method could have found and validated the optimal frequency using less than 180 sample data with 950 sampled data sweeps from 5-100 kHz. The method has less than 1% error of the spotted optimal frequency, compared with the correct optimal frequency. As further research, we interested to enhance the spotting method performance by applying a robust pre-processing method and comparing it with different peak finding algorithms during the initial peak selections. Furthermore, the spotting method optimal frequency tracking and tuning will be being implemented and evaluated with various conditions such as load, coil, and distance alteration.

Chapter 4

A Design Approach to Wireless High-Power Transfer to Multiple Receivers with Asymmetric Circuit

4.1 Background

Wireless Power Transfer (WPT) can supply electric power to an electric device without wires. Nowadays, WPT has been implemented in many practical applications, such as in an electric vehicle [44], biomedical [32] [45], and electronic appliances [46]. The increasing demand for electronic appliances increases the WPT usage since many companies want to avoid complex wire connections. For now and the future challenge, WPT is required to be able to meet the need to charge multiple devices at once [47] [48] [49] [50]. The architecture and optimization fields are considered as a research hotspot in WPT research [11]. The common WPT architecture uses a capacitor compensation on their primary and secondary circuits [5] to achieve high power. Therefore, many works use the idea of resonance as a requirement to obtain the operating frequency [4]. Further, impedance matching [12] and optimization techniques [51] have been proposed to make a high-power WPT system.

The common WPT circuit using the idea of resonance cannot always obtain high power [13]. Adding components to compensate WPT circuit (ex: adding a capacitor in each receiver) can increase the circuit's equivalent series resistance so that it can affect the power and efficiency of the WPT system [16] [17] [18]. Furthermore, the capacitor addition on the multi-receivers WPT becomes more complex along with the increasing number of receivers. For this reason, we propose to use a single capacitor compensation on the primary side of the WPT system. This proposed system can disregard the capacitance parameters and its parasitic resistance on the secondary side. The challenge of exploring this circuit is it lacks symmetry, so it cannot use the idea of resonance. Hence, another approach to achieve high-power optimal operating points needs to be addressed.

In the proposed system, the optimal operating points can be obtained by selecting design variables from the system models depend on the WPT design and system requirements. Therefore, this works challenges the proposed WPT system in three WPT design approaches. Which are 1) Optimal operating capacitance, frequency, and coupling [52]. 2) Optimal operating capacitance, primary coil inductance, and coupling. 3) Optimal capacitance and frequency. Afterward, a problem set is defined based on the selection of design space variables. Since the problem set has multi-objective functions with multi design variables, we use the NSGA-II(Non-dominated Sorting Genetic Algorithm II) [53] to discover the optimal operating points. The NSGA-II has been proven to be effective and fast to solve multi-objective problems in many research fields [9] [54].

In this paper, we present our approach in several steps. Initialized by analyzing the circuit equations, we obtain transfer function as our system model [20] [21] [6]. Our system model contains two transfer functions for each of the load receivers. Thus, both transfer function is used as the objective function and the problem set is defined from the selection of design variables. We confirm our results by conducting LTSPICE simulation for each of the optimization scenarios.

4.2 Proposed Method

4.2.1 System Model

Figure 4.1 shows our proposed WPT circuit, which only uses a single capacitor to transfer power to two receivers. In the primary circuit, the components consist of u as the voltage of voltage source and its voltage resistance R_S , the capacitor (C), the primary coil (L_1) and its parasitic resistance (R_1). The first receiver consists of the first receiver coil (L_2) and its parasitic resistance (R_2), and load (R_{L1}). In the second receiver, the components consist of a second receiver coil (L_3) along with its parasitic resistance (R_3), and load (R_{L2}). The Mutual inductance between the primary circuit with the first receiver is symbolized with M_1 , and the mutual inductance between the primary circuit and the second receiver is notated with M_2 . In this circuit, we also put the cross-coupling mutual inductance between the first and second receiver as M_3 .

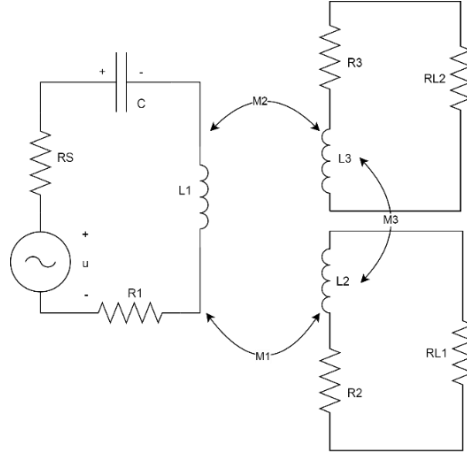


Figure 4.1. Proposed Single Capacitor Dual Receiver WPT Circuit

Using Figure 4.1, we model our system start with the Kirchhoff voltage and current circuit analysis described in (13).

$$\begin{aligned}
 u &= i_1 R_S + i_1 R_1 + L_1 \frac{di_1}{dt} + M_1 \frac{di_2}{dt} + M_2 \frac{di_3}{dt} + v_1 \\
 i_1 &= C \frac{dv_1}{dt} \\
 0 &= i_2 R_{L1} + i_2 R_2 + L_2 \frac{di_2}{dt} + M_1 \frac{di_1}{dt} + M_3 \frac{di_3}{dt}
 \end{aligned} \tag{13}$$

$$0 = i_3 R_{L2} + i_3 R_3 + L_3 \frac{di_3}{dt} + M_2 \frac{di_1}{dt} + M_3 \frac{di_2}{dt}$$

By v_1, i_1, i_2 and i_3 are the state-space variables, u is the input, and y is the output, the state-space representations described as (14).

$$\begin{aligned} \dot{x} &= Ax + Bu \\ y_{L1} &= C_{L1}x + Du \\ y_{L2} &= C_{L2}x + Du \end{aligned} \quad (14)$$

where,

$$\begin{aligned} \begin{bmatrix} \frac{dv_1}{dt} \\ \frac{di_1}{dt} \\ \frac{di_2}{dt} \\ \frac{di_3}{dt} \end{bmatrix} &= A \begin{bmatrix} v_1 \\ i_1 \\ i_2 \\ i_3 \end{bmatrix} + Bu \\ y_{L1} &= C_{L1} \begin{bmatrix} v_1 \\ i_1 \\ i_2 \\ i_3 \end{bmatrix} + Du ; y_{L2} = C_{L2} \begin{bmatrix} v_1 \\ i_1 \\ i_2 \\ i_3 \end{bmatrix} + Du \end{aligned} \quad (15)$$

$$\begin{aligned} C_{L1} &= [0 \quad 0 \quad -R_{L1} \quad 0] \\ C_{L2} &= [0 \quad 0 \quad 0 \quad -R_{L2}] \\ D &= 0 \end{aligned}$$

The transfer-function from u to y_{L1} and y_{L2} are given by:

$$\begin{aligned} G_{L1}(s) &= C_{L1}(sI - A)^{-1}B + D \\ G_{L2}(s) &= C_{L2}(sI - A)^{-1}B + D \end{aligned}$$

$$G_{L1}(s) = \frac{CR_{L1}s^2(M_1R_3 + M_1R_{L2} + s(L_3M_1 - M_2M_3))}{\Delta} \quad (16)$$

$$G_{L2}(s) = \frac{CR_{L2}s^2(M_2R_2 + M_2R_{L1} + s(L_2M_2 - M_1M_3))}{\Delta}$$

where,

$$\begin{aligned} \Delta &= Cs^4(L_1L_2L_3 - L_1M_3^2 - L_2M_2^2 - L_3M_1^2 + 2M_1M_2M_3) + Cs^3(L_1L_2R_3 + L_1L_2R_{L2} + L_1L_3R_2 + L_1L_3R_{L1} + L_2L_3R_1 + L_2L_3R_S - M_1^2R_3 \\ &\quad - M_1^2R_{L2} - M_2^2R_2 - M_2^2R_{L1} - M_3^2R_1 - M_3^2R_S) + R_2R_3 + R_2R_{L2} + R_3R_{L1} + R_{L1}R_{L2} + s^2(CL_1R_2R_3 + CL_1R_2R_{L2} \\ &\quad + CL_1R_3R_{L1} + CL_1R_{L1}R_{L2} + CL_2R_1R_3 + CL_2R_1R_{L2} + CL_2R_3R_S + CL_2R_SR_{L2} + CL_3R_1R_2 + CL_3R_1R_{L1} + CL_3R_2R_S \\ &\quad + CL_3R_SR_{L1} + L_2L_3 - M_3^2) + s(CR_1R_2R_3 + CR_1R_2R_{L2} + CR_1R_3R_{L1} + CR_1R_{L1}R_{L2} + CR_2R_3R_S + CR_2R_SR_{L2} \\ &\quad + CR_3R_SR_{L1} + CR_SR_{L1}R_{L2} + L_2R_3 + L_2R_{L2} + L_3R_2 + L_3R_{L1}) \end{aligned}$$

Using sine wave input (17) (u_0 is the amplitude of the input voltage), we obtain the steady-state voltage formula for the R_{L1} and R_{L2} as y_{ss1} and y_{ss2} described as (18). Next, we describe the formula of steady-state power at R_{L1} and R_{L2} as p_{ss1} and p_{ss2} described in (19).

$$u(t) = u_0 \sin(\omega t) \quad (17)$$

$$\begin{aligned} y_{ss1}(t) &= u_0 |G_{L1}(j\omega)| \sin(\omega t + \angle G_{L1}(j\omega)) \\ y_{ss2}(t) &= u_0 |G_{L2}(j\omega)| \sin(\omega t + \angle G_{L2}(j\omega)) \end{aligned} \quad (18)$$

$$\begin{aligned} p_{ss1}(t) &= \frac{y_{ss1}(t)^2}{R_{L1}} \\ p_{ss2}(t) &= \frac{y_{ss2}(t)^2}{R_{L2}} \end{aligned} \quad (19)$$

4.2.2 Objective function and Optimization

A WPT system can be designed using a couple of coils to deliver power wirelessly. However, this simplest WPT circuit cannot produce high power to the load receivers. Therefore, an additional component needs to be added in the primary or secondary circuit to obtain better power. This method is commonly called the compensation method [8]. Thus, this study adds a single capacitor component on the primary side circuit and calculates the optimal capacitance value to obtain high power.

Common WPT circuit (in Figure 4.2) [5] [4] compensate the system with a capacitor installed on the primary circuit and each receiver's side to obtain high power. Then, the idea of resonance is used to obtain operating frequency (20).

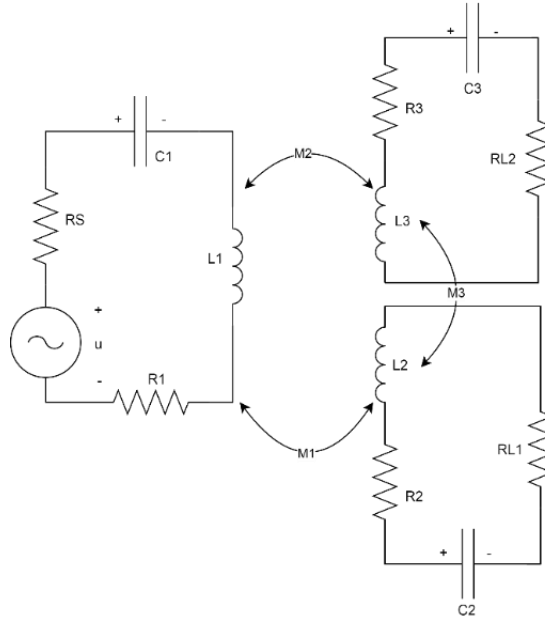


Figure 4.2. Common Dual Receivers WPT Circuit with Capacitor Compensation in Each Receiver.

$$\omega = \frac{1}{\sqrt{L_1 C_1}} = \frac{1}{\sqrt{L_2 C_2}} = \frac{1}{\sqrt{L_3 C_3}} \quad (20)$$

We proposed a method different from the common idea of resonant calculation since our proposed circuit lacks symmetry. Therefore, the optimization approach is needed to be conducted using several choices of the design variables.

4.2.3 Objective Functions

Our study aims for the highest power possible to be absorbed by the load receivers. The objective functions are taken from the steady-state power formulas describes in equation (19). Thus, from (18) to (19), we express our multi-objective function as (21), where f_1 is power absorbed at R_{L1} and f_2 is power absorbed at R_{L2} . The minus sign is given to the expression since the algorithm is using the minimization approach.

$$\begin{aligned} f_1 &= -\frac{|G_{L1}(j\omega)|^2}{R_{L1}} \\ f_2 &= -\frac{|G_{L2}(j\omega)|^2}{R_{L2}} \end{aligned} \quad (21)$$

Equations (21) contain many parameters (13-parameters), and it will be challenging to conduct the optimization using all the parameters. Therefore, it is important to choose the correct design variables during optimization. The WPT design variables were chosen based on the common WPT design requirement and approach, which are:

1. Design a high power WPT to work on the design when the variables selected were capacitance, frequency, and coupling coefficient.
2. Design a high power WPT to work on the design when the variables selected were capacitance, primary coil, and coupling coefficient.
3. Design a high power WPT to work on optimal operating point when the circuit component is fixed except for the capacitor. In this case, the design variables selected were capacitance and frequency.

4.2.4 Design Variables: Capacitance, Frequency, and Coupling Coefficients

Other than capacitance and frequency, the coupling coefficient plays an important part in the WPT system [51] [55]. In our situation, the coupling coefficients K_1 , K_2 and K_3 (as in (22)) are likely to change depends with the gap size between the primary circuit coil and each coil on the receivers [56].

$$K_1 = \frac{M_1}{\sqrt{L_1 L_2}} \quad K_2 = \frac{M_2}{\sqrt{L_1 L_2}} \quad K_3 = \frac{M_3}{\sqrt{L_1 L_2}} \quad (22)$$

The coupling coefficient value is $0 \leq k < 1$ (with the same winding directions of coils). The coupling coefficients can be represented as air gap width between primary and secondary coils [19] the k value approach to zero describes a wide gap situation between coils and vice versa. However, the higher coupling coefficient (or narrow gap) is not always equal to the high power. Our study conducted preliminary computation to get a better representation of this phenomenon. The analysis performed using the equation (21), numerical component values in 0 and $K_1 = K_2$ as free variables. In this computation we assume there is no cross-coupling

between receivers, therefore $K_3=0$. At this preliminary computation we configured the $\omega = 760$ Krad/sec and $C=62.3$ nF.

Table 4.1. Numerical Component value

Parameter	Value	Parameter	Value
L_1	$22 \mu H$	$R_1=R_2=R_3$	0.01Ω
L_2	$11 \mu H$	R_s	1Ω
L_3	$9 \mu H$	R_{L1}, R_{L2}	$8 \Omega, 15 \Omega$

Figure 4.3 shows the result of the computation and present a result where f_1 and f_2 peak is located at some values of $K_1 = K_2$. Therefore, a higher coupling coefficient is not always resulted in high power.

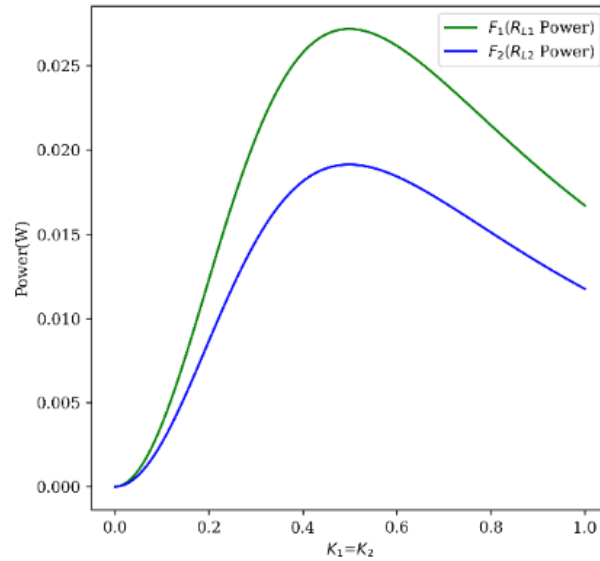


Figure 4.3. Preliminary Computation Results of f_1 and f_2 with Numerical Values in 0 where $K_1 = K_2$ and $K_3=0$

The situation can be complicated if the coupling coefficients $K_1 \neq K_2$. A preliminary computation has been conducted to observe the situation. Using Table 4.1 as the component values, we configured the $\omega = 760$ Krad/sec and $C=62.3$ nF and K_2 is fixed at 0.3 values. Figure 4.4 showed a situation when the second receiver coupling coefficient K_2 is fixed at 0.3, the gap between primary circuit with the first receiver is getting narrower simulated by the K_1 is swept from 0-1. From Figure 4.4 the power at second receiver becomes smaller along the first receiver gap is becomes narrower to the primary circuit. Therefore, in this works, we assume the design meets the optimization requirement where $K_{12} = K_1 = K_2$. Then, we describe the problem set as in (23).

$$\begin{aligned}
& \text{Min } f_1(C, \omega, K_{12}) \\
& \text{Min } f_2(C, \omega, K_{12}) \\
& 1 \text{ pf} \leq C \leq 0.1f \\
& 100 \text{ rad/sec} \leq \omega \leq 1 \cdot 10^9 \text{ rad/sec} \\
& 0.01 \leq K_{12} \leq 0.2
\end{aligned} \tag{23}$$

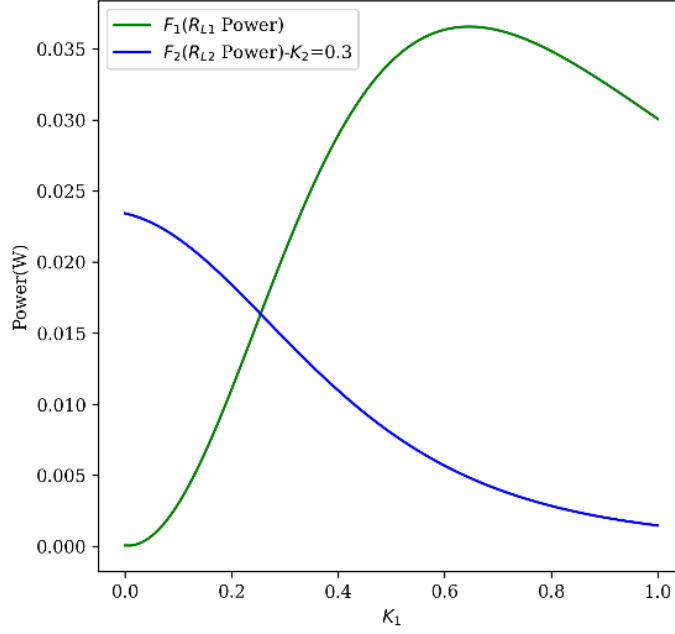


Figure 4.4. Preliminary Computation Results of f_1 and f_2 with Numerical Values in Table 4.1 where K_1 is free variables, $K_2 = 0.3$ and $K_3=0$

4.2.5 Design Variables: Capacitance, Primary Coil, and Coupling Coefficients

Some WPT design requirement is needed to work on ISM (Industrial, Scientific, and Medical) band which 6.78 MHz, 13.56 MHz, and so on [57] [58] [59]. Then, it comes to the fixed frequency. The selection for the others parameter focuses on the primary coils L_1 since the receivers should be in a fixed parameters condition. Therefore, in the ISM band WPT design, we propose to optimize capacitance, primary coil inductance, and coupling coefficients. Then the problem set is defined in (24).

$$\begin{aligned}
& \text{Min } f_1(C, L_1, K_{12}) \\
& \text{Min } f_2(C, L_1, K_{12}) \\
& 1 \text{ pf} \leq C \leq 0.1f \\
& 100 \text{ rad/sec} \leq \omega \leq 1 \cdot 10^9 \text{ rad/sec} \\
& 1 \mu\text{H} \leq L_1 \leq 100 \mu\text{H} \\
& 0.01 \leq K_{12} \leq 0.2
\end{aligned} \tag{24}$$

4.2.6 Design Variables: Capacitance and Frequency

Our optimization also considers an optimization with two selection of design variables, where the selected two variables are the capacitance and frequency. Then, the problem set expresses as in (25).

$$\begin{aligned} & \text{Min } f_1(C, \omega) \\ & \text{Min } f_2(C, \omega) \\ & 1 \text{ pf} \leq C \leq 0.1f \\ & 100 \text{ rad/sec} \leq \omega \leq 1 \cdot 10^9 \text{ rad/sec} \end{aligned} \quad (25)$$

4.2.7 Optimization Tools and Decision Making

We run the optimization using Python Multi-Objective Optimization (PyMOO) [60] by using the NSGA-II. The NSGA-II runs in 500 populations and 200 generations. Since our proposed approach is multi-objective optimization, the solutions can be more than one and result in conflict between objectives. Therefore, a decision to select the best solutions need to be obtained [61].

In this study, we use the pseudo-weight vector approach provided by PyMOO [60] to select the best solutions by configuring the weight of the objectives as in (26) where i is the i -th objective function, x is the design space variables and M is the total of the objective functions.

$$w_i = \frac{(f_i^{\max} - f_i(x))/(f_i^{\max} - f_i^{\min})}{\sum_{m=1}^M (f_m^{\max} - f_m(x))/(f_m^{\max} - f_m^{\min})} \quad (26)$$

Then we decide the best operating point among the optimization solutions, which are selecting the fairest solutions described by giving the pseudo-weight for f_1 and f_2 solutions as 0.5.

4.3 Results and Discussion

4.3.1 Optimization Results with Capacitance, Frequency, and Coupling Coefficients as Design Variables.

In this section, we conducted the optimization by using C , ω , and K_{12} as design variables and problem set in (23) to obtain high power and optimal operating coupling coefficient. By substituting the component values in Table 4.1 to the problem set, we obtained the objective function (27).

$$f_1 = \frac{f_{1n}}{f_d} \quad f_2 = \frac{f_{2n}}{f_d} \quad (27)$$

Where:

$$f_{1n} = -(C^2 K_{12}^2 \omega^4 (1.56 \cdot 10^{-19} \omega^2 + 4.36 \cdot 10^{-7}))$$

$$f_{2n} = -(C^2 K_{12}^2 \omega^4 (3.59 \cdot 10^{-19} \omega^2 + 1.90 \cdot 10^{-7}))$$

$$f_d = -(C^2 \omega^2 (\omega^6 (1.89 \cdot 10^{-29} K_{12}^4 - 1.89 \cdot 10^{-29} K_{12}^2 + 4.74 \cdot 10^{-30})$$

$$+ \omega^4 (2.72 \cdot 10^{-17} K_{12}^4 - 3.03 \cdot 10^{-17} K_{12}^2 + 1.57 \cdot 10^{-17})$$

$$+ \omega^2 (1.267 \cdot 10^{-6} K_{12}^2 + 7.02 \cdot 10^{-6}) + 14.745 \cdot 10^3)$$

$$+ C \omega^2 (\omega^4 (8.62 \cdot 10^{-25} K_{12}^2 - 4.31 \cdot 10^{-25}) + \omega^2 (1.42$$

$$\cdot 10^{-12} K_{12}^2 - 1.42 \cdot 10^{-12}) - 0.63) + 9.8 \cdot 10^{-21} \omega^4$$

$$+ 3.24 \cdot 10^{-8} \omega^2 + 14.455 \cdot 10^3))$$

The optimization results are presented in 0, where the NSGA-II obtained a total of 18 solutions. The results of the decision making shown in 0Afterward, The LTSPICE simulations were conducted to confirm the TABLE II Results. The simulations ran in the AC analysis with 1-Volts source voltage. The results from the LTSPICE are processed and plotted using Python in 0.

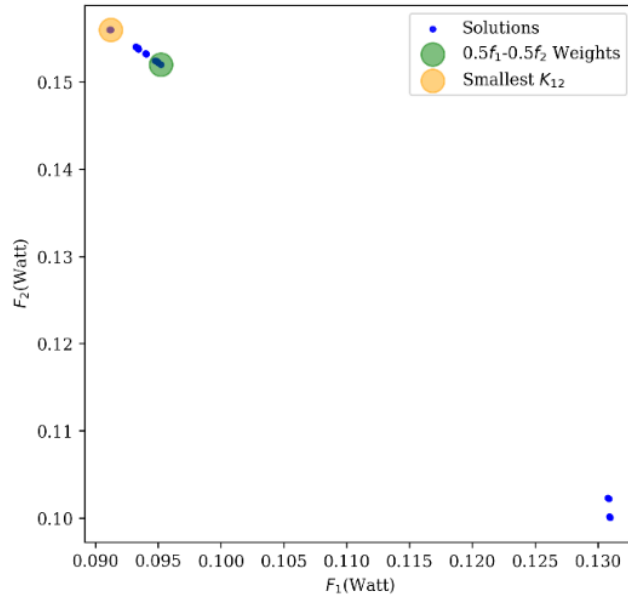


Figure 4.5. Optimization Results for objective functions in equation (27) Using Numerical Values in 0 where $K_{12} = K_1 = K_2$ and $K_3 = 0$

Table 4.2. Figure 4.5 Decision Making Results

Decision Making	Objective Values		Design Values		
	f_1 (Watt)	f_2 (Watt)	C (F)	Frequency (Hertz)	K_{12}
Pseudo-Weight $0.5-f_1$	0.09	0.15	10.2n	343.01 k	0.16

Decision Making	Objective Values		Design Values		
	f_1 (Watt)	f_2 (Watt)	C (F)	Frequency (Hertz)	K_{12}
0.5- f_2					
Smallest K_{12}	0.09	0.15	7.78 n	392.95 k	0.15

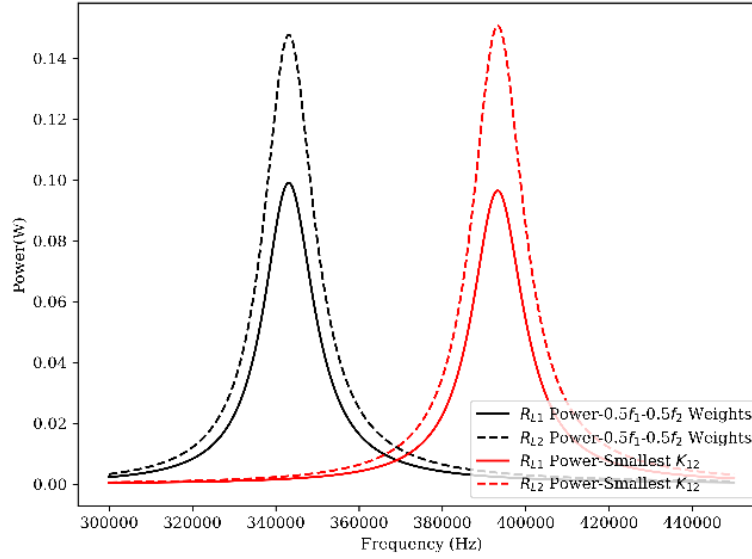


Figure 4.6. LTSPICE Results Plotted using Python for obtained design values in Table 4.2.

4.3.2 Optimization Results with Capacitance, Primary Coil and Coupling Coefficients as Design Variables.

In this section, the optimization conducted when the frequency is fixed at 6.78 MHz, and the design variables chosen were C , L_1 , and K_{12} . The optimization is conducted using the component values in the Table 4.1 except for the L_1 will be treated as the design variables.

By substituting the component values to Table 4.1 with frequency 6.78MHz to the problem set (24), we obtained the objective function in (28).

$$f_1 = \frac{f_{1n}}{f_d} \quad f_2 = \frac{f_{2n}}{f_d} \quad (28)$$

Where:

$$f_{1n} = -(4.253 \cdot 10^{31} C^2 K_{12}^2 L_1)$$

$$f_{2n} = -(9.736 \cdot 10^{31} C^2 K_{12}^2 L_1)$$

$$f_d = -(4.238 \cdot 10^{41} C^2 K_{12}^4 L_1^2 - 4.238 \cdot 10^{41} C^2 K_{12}^2 L_1^2 + 2.828 \cdot 10^{32} C^2 K_{12}^2 L_1 + 1.06 \cdot 10^{41} C^2 L_1^2 + 5.968 \cdot 10^{25} C^2 + 2.338 \cdot 10^{26} C K_{12}^2 L_1 - 1.17 \cdot 10^{26} C L_1 + 3.227 \cdot 10^{10})$$

The optimization generates single solutions shown in 0. Using the optimum value in capacitance, primary coil inductance, and coupling coefficients in TABLE III, we conducted the AC analysis with a 1-Volts voltage source simulation in LTSPICE. The results were plot using Python as in 0.

Table 4.3. Decision Making Results

Objective Values		Design Values		
f_1 (Watt)	f_2 (Watt)	C (F)	L_1 (H)	K_{12}
0.09	0.15	56.2p	10.65μ	0.19

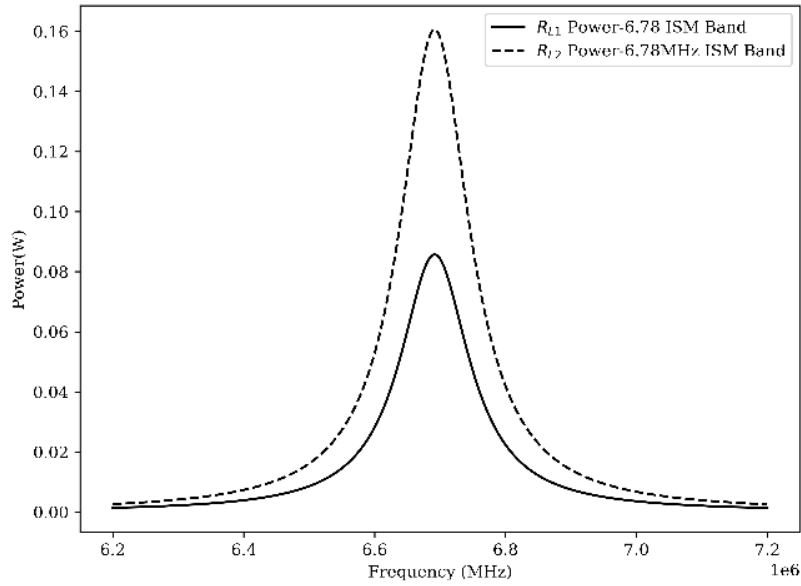


Figure 4.7. LTSPICE Results Plotted using Python for obtained design values in 0

4.3.3 Optimization Results with Capacitance and Frequency Design Variables.

In this sub-section, we present results when the optimization considers only two design variables: capacitance (C) and frequency (ω). The numerical values for other components are shown in Table 4.4.

Table 4.4. Component values for optimization with capacitance and frequency as design variables

Parameter	Value	Parameter	Value
L_1	22 μH	K_2	0.12
L_2	11 μH	K_3	0
L_3	9 μH	R_s	1 Ω
$R_1=R_2=R_3$	0.01 Ω	R_{L1}	8 Ω
K_1	0.09	R_{L2}	15 Ω

By substitute the component values from Table 4.4 to equation(25), we obtain the second scenario objective function. The f_1 is representing power at load R_{L1} , and described in equation (29).

$$f_1 = \frac{f_{1n}}{f_d} \quad f_{2d} = \frac{f_{2n}}{f_d}$$

Where:

$$\begin{aligned} f_{1n} &= -(C^2\omega^4(1.556 \cdot 10^{-21}\omega^2 + 4.33 \cdot 10^{-9})) \\ f_{2n} &= -(C^2\omega^4(5.245 \cdot 10^{-21}\omega^2 + 2.781 \cdot 10^{-9})) \\ f_d &= -C^2\omega^2(4.513 \cdot 10^{-30}\omega^6 + 1.54 \cdot 10^{-17}\omega^4 + 7.043 \cdot 10^{-6}\omega^2 + 14.745 \cdot 10^3) \\ &\quad - C\omega^2(4.206 \cdot 10^{-25}\omega^4 + 1.412 \cdot 10^{-12}\omega^2 + 0.636) + 9.801 \\ &\quad \cdot 10^{-21}\omega^4 + 3.245 \cdot 10^{-8}\omega^2 + 14.455 \cdot 10^3 \end{aligned} \quad (29)$$

The optimization performed using NSGA-II by configuring the population size 500 and 200 generations. The results obtained by NSGA-II from PyMOO tools, showing 192 solutions, as presented in 0.

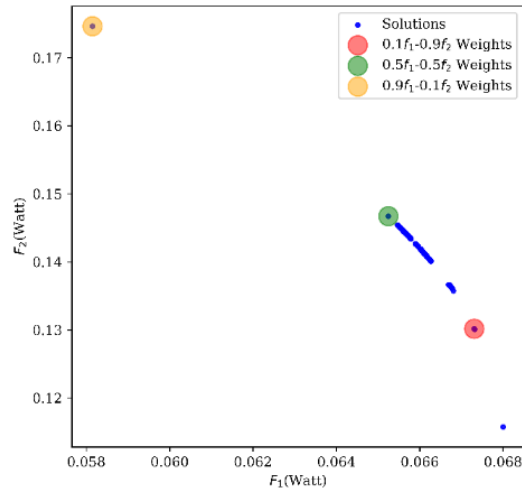


Figure 4.8. Optimization Results for objective functions in equation (29) Using Numerical Values in Table 4.4.

Table 4.5. Figure 4.8 Decision Making Results

Decision Making	Objective Values		Design Values	
	f_1 (Watt)	f_2 (Watt)	C (F)	Frequency (Hertz)
Pseudo-Weight $0.1-f_1$ $0.9-f_2$	0.06	0.13	18.45n	251.93k
Pseudo-Weight $0.5-f_1$ $0.5-f_2$	0.06	0.14	11.6n	317.95k
Pseudo-Weight $0.9-f_1$ $0.1-f_2$	0.05	0.17	2.59n	674.74k

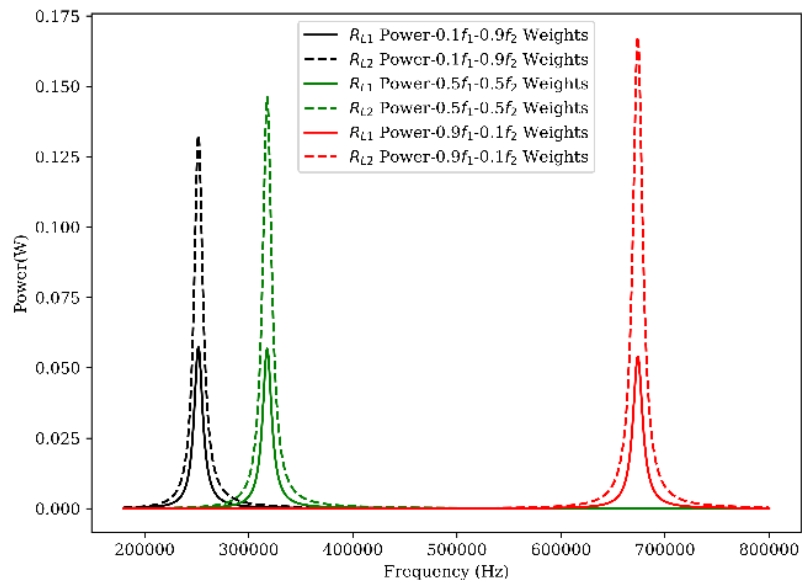


Figure 4.9. LTSPICE Results Plotted using Python for obtained design values in Table 4.5.

4.3.4 Comparison Between Proposed WPT Circuit with The Common WPT circuit.

This study compares the proposed circuit in Figure 4.1 with the common WPT circuit in Figure 4.2 using the component configuration in Table 4.6 was taken from research in [47].

Table 4.6. Component values for scenario 1

Parameter	Value
$L_1=L_2=L_3$	22 μH
$R_1=R_2=R_3$	0.01 Ω
$M_1=M_2$	5 μH
M_3	0
R_s	1 Ω
$R_{L1} = R_{L2}$	8 Ω

By substituting the component from Table 4.6 to equation (21), we obtain the objective function (30). The f_1 and f_2 value component is equal since both receivers have the same component values.

$$f_1 = \frac{f_{1n}}{f_d} \quad f_2 = f_1$$

$$f_{1n} = 8C^2\omega^4(1.21 \cdot 10^{-20}\omega^2 + 1.60 \cdot 10^{-9}) \quad (30)$$

$$f_{1d} = C^2(9.11 \cdot 10^{-29}\omega^8 + 2.77 \cdot 10^{-17}\omega^6 + 2.11 \cdot 10^{-6}\omega^4 + 4.199 \cdot 10^3\omega^2) + C(-9.24 \cdot 10^{-24}\omega^6 - 2.59 \cdot 10^{-12}\omega^4 - 0.18\omega^2) + 2.34 \cdot 10^{-19}\omega^4 + 6.21 \cdot 10^{-8}\omega^2 + 4.116 \cdot 10^3$$

We run the optimization using Python Multi-Objective Optimization (PyMOO) by configured the population size 500 and 200 generations. The results obtained are $C = 21.4$ nF and $freq = 243.89$ kHz with $f_1 = f_2 = 0.12$ Watt. For the common WPT circuit in Figure 4.2, we are using the idea of resonance calculations using equations (20) by configuring $C_1 = C_2 = C_3 = 110$ nF and frequency = 102 kHz.

The simulation results for the proposed circuit are plotted in 0, and the results show 0.12-Watt power obtained by both R_{L1} and R_{L2} . Next, we simulated the idea of resonance calculation on common The LTSPICE simulations ran on using AC analysis with frequency swept from 50-150 kHz. The simulations results are plotted in 0, where 0.10-Watt power obtained by the R_{L1} and R_{L2} at optimum frequency.

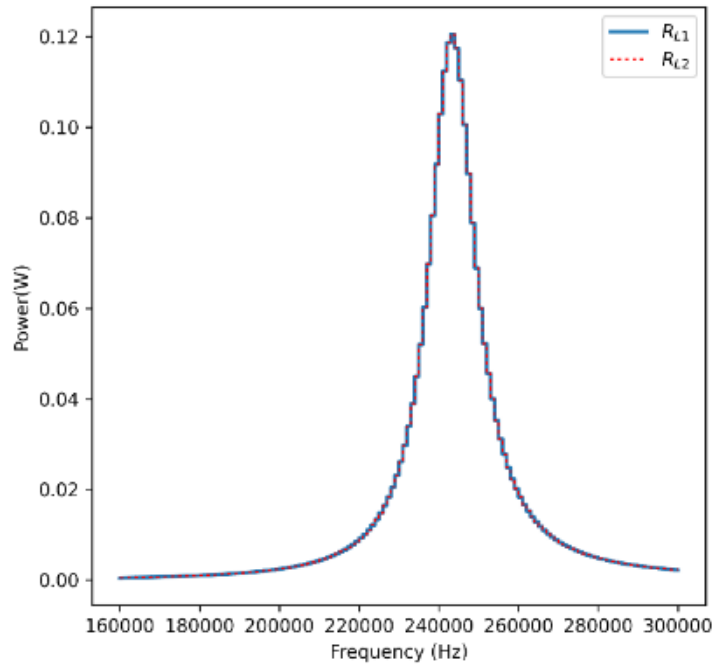


Figure 4.10. Power at R_{L1} and R_{L2} using proposed circuit and optimization method with $C=21.4$ nF and $freq=243.89$ kHz (Obtained from LTSPICE simulations)

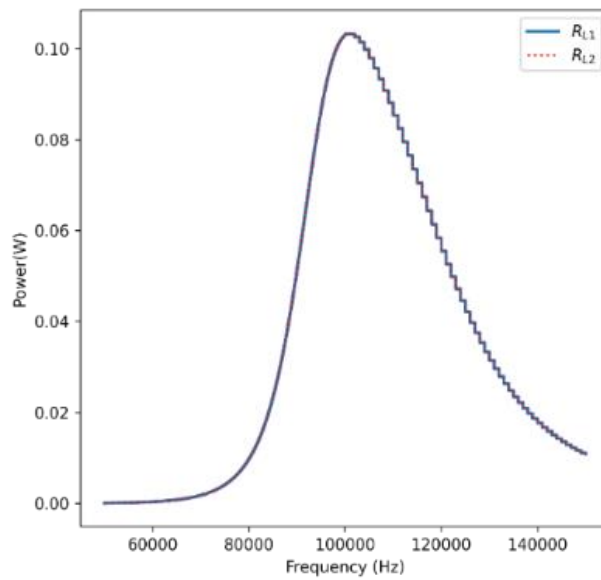


Figure 4.11. Power at R_{L1} and R_{L2} in Fig.2. circuit and idea of resonance calculation using $C_1 = C_2 = C_3 = 110$ nF. (Obtained from LTSPICE simulations)

4.3.5 Discussions

This study presented a high power WPT system using single capacitor compensation on the primary circuit. A system model has been obtained from the system transfer function. The objective function is obtained through the system model and tested using several design spaces to answer the WPT design challenges. The optimization is conducted with PyMOO tools with NSGA-II using 500 populations and 200 generations. Since the optimization conducted using two objective functions, the obtained solutions can be more than one. Therefore, a decision making using fair $0.5f_1-0.5f_2$ pseudo-weight is chosen. If there are changes in priority due to the system requirements, the weight can be changed as in Figure 4.9. Then the LTSPICE simulation conducted using the AC analysis using 1-Volt source voltage and plotted using Python programming.

Table 4.7. Design Spaces Comparison Result

Design Spaces	Optimum Objective Values		Optimum Design Values
	f_1 (Watt)	f_2 (Watt)	
C, ω, K_{12} Pseudo-weight= $0.5f_1-0.5f_2$	0.09	0.15	$C=10.2\text{nF}$ freq= 343.01 kHz $K_{12}=0.16$
C, L_1, K_{12}	0.09	0.15	$C=56.2\text{pF}$ $L_1=10.65\mu\text{H}$ $K_{12}=0.19$
C, ω Pseudo-weight= $0.5f_1-0.5f_2$	0.06	0.14	$C=11.6\text{nF}$ freq =317.95kHz

The optimization results on the three design space variables (C, ω, K_{12} and C, L_1, K_{12}) showing all solutions have a 0.14 -Watt summation from f_1 and f_2 . The conclusion for both optimization results shown in Table 4.7. By comparing the total optimum objective values in f_1 and f_2 for every solution on design variables scenario, it can be concluded the optimum value can be obtained from the three choices of design spaces, which are C, ω, K_{12} and C, L_1, K_{12} . Compared with the common WPT circuit, this study conducted a comparison using the same component values except for the capacitor and frequency components. Our results show better power able to be absorbed by both receivers. The common WPT circuit with the idea of resonance and selected capacitor and frequency values is not working on the operational point conditions. Therefore, even though resonance can be calculated using equations (20), the optimal operating points discovery should be considered in any kind of circuit to obtain high power.

This study uses the running metric analysis [62] to observe whether the number of generations satisfies the optimization result. The running metric analysis is conducted since the true Pareto front of our objective function is not known. The results of the running metric analysis are observed in Figure 4.12. The results show that the objective function difference is closer when the optimization run in the 160-200 generations. Therefore, this study chooses the 200 generations.

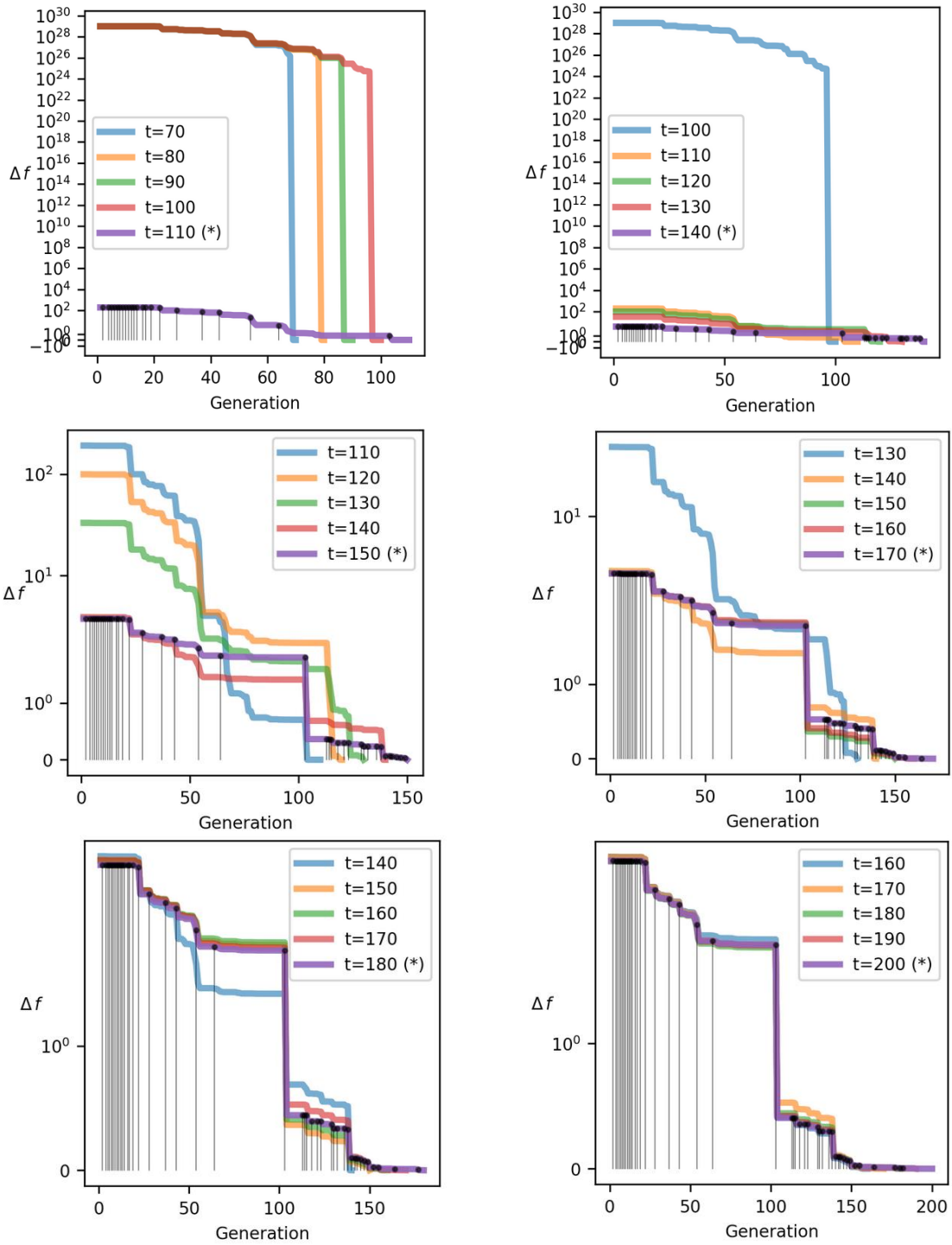


Figure 4.12 Running Metrics Analysis

This study also observed the time execution during the optimization process. The time execution conducted using pseudo-code below:

```

start_time = time.time()

problem = MyProblem()

algorithm = NSGA2(pop_size=500)

res = minimize(problem,
               algorithm,
               ("n_gen", 200),
               verbose=False,
               seed=1)

end_time = time.time()

print("Elapsed time:",end_time-start_time)

```

The experiment was conducted ten times on every optimization process in the optimization scenario mentioned in the sub-chapters 4.3.1, 4.3.2, and 4.3.5. The result of the time analysis is shown in Table 4.8.

Table 4.8. Optimization Time

Experiment	4.3.1 Elapsed Time (seconds)	4.3.2 Elapsed Time (seconds)	4.3.3 Elapsed Time (seconds)
1	39.41	31.65	27.28
2	36.81	33.70	27.28
3	45.28	30.94	26.76
4	39.44	31.44	26.82
5	44.26	29.21	27.21
6	53.9	28.39	26.73
7	44.41	31.43	27.16
8	38.49	31.87	26.92
9	34.92	31.03	26.91
10	36.67	31.69	26.79
Avg	41.36	31.14	26.99

The proposed approach is currently focused on a series-series WPT circuit from the optimization of components design variables. Whereas there are possibilities, higher power

can be achieved at some operating points on other forms of architecture. In the future, the mathematical model in the other forms of architecture can be derived using our approach in obtaining transfer function. Then, the optimal high-power operating points can be compared between architectures in order to get the highest power WPT system.

Our current system is supplied by one voltage source with one frequency. In the future, it is also important to consider whether each of the load receiver able to absorb power delivered using many frequencies from many voltage sources. Therefore, our current system model should be improved by adding multi-frequency source analysis.

4.4 Conclusions

In this paper, we proposed a high-power WPT system with single capacitor compensation on the primary side. Our approach initialized with the derivation of the mathematical system model. The system model consists of two load receivers transfer functions to be used in the objective function. The problem set is defined from the selection of design variables and optimized using NSGA-II. The optimization has been conducted in three WPT design variables selection, which are: 1) Optimal operating capacitance, frequency, and coupling. 2) Optimal operating capacitance, primary coil inductance, and coupling. 3) Optimal capacitance and frequency.

The optimization results show that the three design space variables selection (C, ω, K_{12} and C, L_1, K_{12}) have a maximum power achieved (0.14-Watt). Based on the experiment, the proposed system load receivers absorbed higher power than the common WPT circuit using the idea of resonance by 20%. Therefore, our proposed system's optimal operating points are achieved, even though our proposed system lacks symmetry and not using the ideas of resonance.

Chapter 5 Summary

This study main objectives are conducting investigation for common symmetry WPT circuit and its method to deliver high-power using the idea of resonance. By applying system model and analyzed the behavior of the system through frequency response, it has been found whether the idea to deliver high-power using resonant frequency is not accurate. Reasons and alternative solutions concluded as follow:

1. The theoretical computation and investigation have been conducted to observe the method to deliver high-power using symmetric circuit and the idea of resonance. Based on the frequency response, the idea of resonance in the symmetric circuit is only valid at some coupling coefficient value. The optimal operating frequency to deliver high-power during the changes of coupling coefficient (gap/misalignment) is shifted from the frequency resonant calculation.
2. This study provides a solution to obtain operating frequency to deliver high-power to secondary circuit in without the idea of resonance by conducted based on a frequency sweeping improvement. Although it is theoretically possible to determine the optimal frequency by wide range frequency sweep, it is practically important to spot it in a few trials of frequency. Hence, this study presents a frequency spotting strategy using a square wave input power signal. The method is implementing Fourier analysis of the response stimulated by the square wave input signals. Therefore, an alternative peak other than the global peak can be selected if the system has frequency restrictions. This strategy avoids a long time-consuming sweeping process with knowledge of response by square wave input. The Automatic Multiscale-based Peak Detection (AMPD) algorithm is applied to select the initial peak finding on every data sample increment iteration to further analysis to find the set of peak patterns by calculating error parameters.
3. This study has been presented an approach the deliver wireless high-power transfer on asymmetric circuit (capacitance-less receiver circuit). It should be noticed that an additional component compensation on the common WPT circuit increases the system's equivalent series resistance and affect the power and efficiency absorbed by the load receivers. The complexity of the system will increase along with the increasing number of receivers. Thus, in this works, we explore the WPT circuit that only compensated with the primary side capacitor in transferring high power to dual receivers. Using one capacitor on the primary side makes the circuit lacks symmetry, so it cannot use the idea of resonance. Therefore, to discover high power operating points, we use an optimization approach. This study presented several design variables optimization approaches to obtain high power operating point. The NSGA-II (Non-dominated Sorting Genetic Algorithm II) is used to optimize the mathematical system model's design variables. The results show that the proposed system can obtain high power even though using only a single capacitor compensation without the idea of resonance. The

optimization results show that the three design space variables selection (C, ω, K_{12} and C, L_1, K_{12}) have a maximum power achieved (0.14-Watt). Based on the experiment, the proposed system load receivers absorbed higher power than the common WPT circuit using the idea of resonance by 20%. Therefore, our proposed system's optimal operating points are achieved, even though our proposed system lacks symmetry and not using the ideas of resonance.

Our study finds whether the idea of resonance and symmetric circuit are not always able to deliver high-power. This study presented that the high-power can be delivered even though without the idea of resonance, or without using the symmetric circuit. For the future works, the real-time estimation of gap/coil misalignment should be conducted to know the coupling coefficients estimation. This method can be conducted by comparing the results of sweeping using our fast-spotting algorithm and the results of the model computation that collect the data from several coupling coefficient values. By understanding the current coupling coefficient value, the circuit can be compensated by some primary capacitor values that can be obtained using optimization such as our proposed approach.

References

- [1] N. Tesla, "Apparatus For Transmitting Electrical Energy". US Patent 1119732, 1 December 1914.
- [2] Wireless Power Consortium, "Qi-Mobile Computing | Wireless Power Consortium," [Online]. Available: <https://www.wirelesspowerconsortium.com/qi/>. [Accessed 5 2021].
- [3] A. M. Jawad, R. Nordin, S. K. Gharghan, H. M. Jawad and M. Ismail, "Opportunities and Challenges for Near-Field Wireless Power Transfer: A Review," *Energies*, vol. 10, no. 1022, pp. 1-28, 2017.
- [4] X. Mou and H. Sun, "Wireless Power Transfer: Survey and Roadmap," in 2015 IEEE 81st Vehicular Technology Conference (VTC Spring), Glasgow, 2015.
- [5] S. Y. R. Hui, W. Zhong and C. K. Lee, "A Critical Review of Recent Progress in Mid-Range Wireless Power Transfer," *IEEE Transactions on Power Electronics*, vol. 29, no. 9, 2014.
- [6] K. Yamaguchi, T. Hirata and I. Hodaka, "High Power Wireless Power Transfer Driven by Square Wave Inputs," in Genetic and Evolutionary Computing. GEC 2015. Advances in Intelligent Systems and Computing, Yangon, Myanmar , 2015.
- [7] K.N.Mude and K. Aditya, "Comprehensive review and analysis of two-element resonant compensation topologies for wireless inductive power transfer systems," *Chinese Journal of Electrical Engineering*, vol. 5, no. 2, pp. 14-31, 2019.
- [8] W. Zhang and C. C. Mi, "Compensation Topologies of High-Power Wireless Power Transfer Systems," *IEEE Transactions on Vehicular Technology*, pp. 4768 - 4778, 2015.
- [9] S. G. Manuele Bertoluzzo and E. Sieni, "Automatic Optimization of the Compensation Networks of a Wireless Power Transfer System," *Energies*, vol. 13, no. 20, 2020.
- [10] C. Jiang, K. T. Chau, C. Liu and C. H. T. Lee, "An Overview of Resonant Circuits for Wireless Power Transfer," *Energies*, vol. 10, no. 894, 2017.
- [11] X. Wei, Z. Wang and H. Dai, "A Critical Review of Wireless Power Transfer via Strongly Coupled Magnetic Resonances," *Energies*, vol. 7, no. 7, pp. 4316-4341, 2014.
- [12] T. C. Beh, M. Kato, T. Imura, S. Oh and Y. Hori, "Automated Impedance Matching System for Robust Wireless Power Transfer via Magnetic Resonance Coupling," *IEEE Transactions on Industrial Electronics*, vol. 60, no. 9, pp. 3689-3698, 2013.
- [13] K. Yamaguchi, T. Hirata, Y. Yamamoto and I. Hodaka, "Resonance and efficiency in wireless power transfer system," in *WSEAS Transactions on Circuits and Systems*, 2014.
- [14] V. Jiwariyavej, T. Imura and Y. Hori, "Coupling Coefficients Estimation of Wireless Power Transfer System via Magnetic Resonance Coupling Using Information From Either Side of the System," *IEEE Journal of Emerging and Selected Topics in Power Electronics*, vol. 3, no. 1, pp. 191-200, 2015.
- [15] K. Yamaguchi, I. Hodaka and Y. Yamamoto, "Estimation of Coupling Coefficient for Wireless Power Transfer," in the 12th International Conference on Electronics, Hardware, Wireless and Optical Communications (EHAC '13), Cambridge, 2013.
- [16] X. Liu, L. Clare, X. Yuan, C. Wang and J. Liu, "A Design Method for Making an LCC Compensation Two-Coil Wireless Power Transfer System More Energy Efficient Than an SS Counterpart," *Energies*, vol. 10, no. 9, p. 1346, 2017.

- [17] C. Cheng, Z. Zhou, W. Li, C. Zhu, Z. Deng and C. C. Mi, "A Multi-Load Wireless Power Transfer System With Series-Parallel-Series Compensation," *IEEE Transactions on Power Electronics*, vol. 34, no. 8, pp. 7126 - 7130, 2019.
- [18] H. Qiang, X. L. Huang, L. Tan, Q. Ji and J. M. Zhao, "Achieving maximum power transfer of inductively coupled wireless power transfer system based on dynamic tuning control," *Science China Technological Sciences*, vol. 55, p. 1886–1893, 2012.
- [19] Y. Yang, J. Cui and X. Cui, "Design and Analysis of Magnetic Coils for Optimizing the Coupling Coefficient in an Electric Vehicle Wireless Power Transfer System," *Energies*, vol. 13, p. 4143, 2020.
- [20] T. Hirata, K. Yamaguchi and I. Hodaka, "A symbolic equation modeler for electric circuits," *ACM Communications in Computer Algebra*, vol. 49, no. 3, pp. 1932-2240, 2015.
- [21] K. Yamaguchi, T. Hirata and I. Hodaka, "A general method to parameter optimization for highly efficient wireless power transfer," *International Journal of Electrical and Computer Engineering*, vol. 6, no. 6, pp. 3217-3221, 2016.
- [22] E. Setiawan, T. Hirata and I. Hodaka, "Accurate Symbolic Steady State Modeling of Buck Converter," *International Journal of Electrical and Computer Engineering*, vol. 7, no. 5, p. 2374 – 2381, 2017.
- [23] S. D. Barman, A. W. Reza, N. Kumar and M. E. Karim, "Wireless powering by magnetic resonant coupling: Recent trends in wireless power transfer system and its applications," *Renewable and Sustainable Energy Reviews*, vol. 51, pp. 1526-1552, 2015.
- [24] G. C. Abner Ramirez, "Reduced-sample numerical Laplace transform for transient and steady-state simulations: Application to networks involving power electronic converters," *International Journal of Electrical Power & Energy Systems*, vol. 109, pp. 480-494, 2019.
- [25] W. A. Wolovich, *Automatic Control Systems: Basic Analysis and Design*, Oxford University Press, Inc., 1993.
- [26] S. Chhawchharia, S. K. Sahoo, M. Balamurugan, S. Sukchai and F. Yanine, "Investigation of wireless power transfer applications with a focus on renewable energy," *Renewable and Sustainable Energy Reviews*, vol. 91, pp. 888-902, 2018.
- [27] D. Kim, A. Abu-Siada and A. Sutinjo, "State-of-the-art literature review of WPT: Current limitations and solutions on IPT," *Electric Power Systems Research*, vol. 154, pp. 439-502, 2018.
- [28] A. Kurs, A. Karalis, R. Moffatt, J. D. Joannopoulos, P. Fisher and M. Soljacic', "Wireless Power Transfer via Strongly Coupled Magnetic Resonances," *Science*, vol. 317, pp. 83-86, 2007.
- [29] A. El-Shahat, E. Ayisire, Y. Wu, M. Rahman and D. Nelms, "Electric Vehicles Wireless Power Transfer State-of-The-Art," *Energy Procedia*, vol. 162, pp. 24-37, 2019.
- [30] H. Hoang, S. Lee, Y. Kim, Y. Choi and F. Bien, "An Adaptive Technique to Improve Wireless Power Transfer for Consumer Electronics," *IEEE Transactions on Consumer Electronics*, vol. 58, no. 2, pp. 327-332, 2012.
- [31] L. Han and L. Li, "Integrated wireless communications and wireless power transfer: An Overview," *Physical Communication*, vol. 25, pp. 555-563, 2017.
- [32] H.-J. Kim, H. Hirayama, S. Kim, K. J. Han, R. Zhang and J.-W. Choi, "Review of Near-Field Wireless Power and Communication for Biomedical Applications," *IEEE Access*, vol. 5, pp. 21264 - 21285, 2017.
- [33] M. Zargham and P. G. Gulak, "Maximum Achievable Efficiency in Near-Field Coupled Power-Transfer Systems," *IEEE TRANSACTIONS ON BIOMEDICAL CIRCUITS AND SYSTEMS*, vol. 6, no. 3, pp. 228-243, 2012.

- [34] Y. Cheng, D. Xuan, X. Su, W. Wu and G. Wang, "An optimal operating frequency selection scheme for maximizing inductive power link efficiency," *Microwave and Optical Technology Letters*, vol. 60, p. Microw Opt Technol Lett, 2018.
- [35] X. Dai, X. Li, Y. Li and A. P. Hu, "Maximum Efficiency Tracking for Wireless Power Transfer Systems With Dynamic Coupling Coefficient Estimation," *IEEE TRANSACTIONS ON POWER ELECTRONICS*, vol. 33, no. 6, pp. 5005-5015, 2018.
- [36] D. Patil, M. Sirico, L. Gu and B. Fahimi, "Maximum Efficiency Tracking in Wireless Power Transfer for Battery Charger: Phase Shift and Frequency Control," in *IEEE Energy Conversion Congress and Exposition (ECCE)*, Milwaukee, 2016.
- [37] N. Kim, K. Kim, J. Choi and C.-W. Kim, "Adaptive frequency with power-level tracking system for efficient magnetic resonance wireless power transfer," *Electronics Letters*, vol. 48, no. 8, pp. 452-454, 2012.
- [38] S. Ahmet and S. KAVUT, "A frequency-tuned magnetic resonance-based wireless power transfer system with A frequency-tuned magnetic resonance-based wireless power transfer system with," *Turkish Journal of Electrical Engineering & Computer Sciences*, vol. 26, p. 3168 – 3180, 2018.
- [39] C. Özdemir and A. N. Mete, "A Frequency-Tracking Algorithm for Inductively Coupled Wireless Power Transfer Systems," in *International Conference on Electrical and Electronics Engineering (ELECO)*, Bursa, Turkey, 2017.
- [40] K. Yamaguchi, T. Hirata and I. Hodaka, "Using Square Wave Input for Wireless Power Transfer," *International Journal of Electrical and Computer Engineering (IJECE)*, vol. 6, no. 1, p. 431 – 438, 2016.
- [41] F. Scholkmann, J. Boss and M. Wolf, "An Efficient Algorithm for Automatic Peak Detection in Noisy Periodic and Quasi-Periodic Signals," *Algorithms*, vol. 5, pp. 588-603, 2012.
- [42] A. M. Colak, T. Manabe, Y. Shibata and F. Kurokawa, "Peak Detection Implementation for Real-Time Signal Analysis Based on FPGA," *Circuits and Systems*, vol. 9, pp. 148-167, 2018.
- [43] T.-C. Huang and Y.-M. Wu, "A Robust Algorithm for Automatic P-wave Arrival-Time Picking Based on the Local Extrema Scalogram," *Bulletin of the Seismological Society of America*, vol. 109, no. 1, p. 413-423, 2019.
- [44] L. Sun, D. Ma and HoujunTang, "A review of recent trends in wireless power transfer technology and its applications in electric vehicle wireless charging," *Renewable and Sustainable Energy Reviews*, vol. 91, pp. 490-503, 2018.
- [45] S. Kokosis, E. Gati, N. Patsourakis and S. Manias, "Comparative evaluation of GaN transistors and Si MOSFETs for use in inductive power transfer systems of biomedical implantable devices," *WSEAS Transactions on Power Systems*, vol. 14, pp. 172-180, 2019.
- [46] M.-F. STAN, N. FIDEL, I. MINA and A.-G. HUSU, "Improvement of Wireless Power Transfer Efficiency for Home Electronics and Appliances with the Use of SMD Components," in *2018 10th International Conference on Electronics, Computers and Artificial Intelligence (ECAI)*, Iasi, Romania, 2018.
- [47] W. Cai, D. Ma, H. Tang, X. Lai, X. Liu and L. Sun, "Highly Efficient Target Power Control for Two-Receiver Wireless Power Transfer Systems," *Energies*, vol. 11, no. 10, p. 2726, 2018.
- [48] K. Zhuo, B. Luo, Y. Zhang and Y. Zuo, "Multiple receivers wireless power transfer systems using decoupling coils to eliminate cross-coupling and achieve selective target power distribution," *IEICE Electronics Express*, vol. 16, no. 18, p. 20190491, 2019.

- [49] M. WAGIH, A. KOMOLAFE and B. ZAGHARI, "Dual-Receiver Wearable 6.78 MHz Resonant Inductive Wireless Power Transfer Glove Using Embroidered Textile Coils," *IEEE Access*, vol. 8, pp. 24630-24642, 2020.
- [50] W. Cai, D. Ma, X. Lai, K. H. H. Tang and J. Xu, "Time-Sharing Control Strategy for Multiple-Receiver Wireless Power Transfer Systems," *Energies*, vol. 13, no. 3, p. 599, 2020.
- [51] M. Frivaldsky, V. Jaros, P. Spanik and M. Pavelek, "Control system proposal for detection of optimal operational point of series-series compensated wireless power transfer system," *Electrical Engineering*, vol. 102, p. 1423-1432, September 2020.
- [52] D.-W. Seo, J.-H. Lee and a. H.-S. Lee, "Optimal Coupling to Achieve Maximum Output Power in a WPT System," *IEEE TRANSACTIONS ON POWER ELECTRONICS*, vol. 31, no. 6, pp. 3994-3998, 2016.
- [53] K. Deb, A. Pratap, S. Agarwal and T. Meyarivan, "A fast and elitist multiobjective genetic algorithm: NSGA-II," *IEEE Transactions on Evolutionary Computation*, vol. 6, no. 2, pp. 182-197, 2002.
- [54] M. M. Farizhendy, E. Noorzai and M. Golabchi, "Implementing the NSGA-II genetic algorithm to select the optimal repair and maintenance method of jack-up drilling rigs in Iranian shipyards," *Ocean Engineering*, vol. 211, p. 107548, 2020.
- [55] S. Chatterjee, A. Iyer, C. Bharatiraja, I. Vaghasia and V. Rajesh, "Design Optimisation for an Efficient Wireless Power Transfer System for Electric Vehicles," *Energy Procedia*, vol. Volume 117, pp. 1015-1023, 2017.
- [56] Y. Li, S. Jiang, X.-L. Liu, Q. Li, W.-H. Dong, J.-M. Liu and X. Ni, "Influences of Coil Radius on Effective Transfer Distance in WPT System," *IEEE Access*, vol. 7, pp. 125960-125968, 2019.
- [57] L. Gu, G. Zulauf, A. Stein, P. A. Kyaw, T. Chen and J. M. R. Davila, "6.78-MHz Wireless Power Transfer With Self-Resonant Coils at 95% DC-DC Efficiency," *IEEE Transactions on Power Electronics*, vol. 36, no. 3, pp. 2456-2460, March 2021.
- [58] J. Song, M. Liu and C. Ma, "Analysis and Design of A High-Efficiency 6.78-MHz Wireless Power Transfer System With Scalable Number of Receivers," *IEEE Transactions on Industrial Electronics*, vol. 67, no. 10, pp. 8281-8291, 2020.
- [59] M. Wagih, A. O. Komolafe and B. Zaghari, "Position Independent Wearable 6.78 MHz Near-Field Radiative Wireless Power Transfer using Electrically-Small Embroidered Textile Coils," in *2019 19th International Conference on Micro and Nanotechnology for Power Generation and Energy Conversion Applications (PowerMEMS)*, 1-5, 2019.
- [60] J. Blank and K. Deb, "Pymoo: Multi-Objective Optimization in Python," *IEEE Access*, vol. 8, pp. 89497-89509, 2020.
- [61] K. Deb, "Multi-Objective Optimization Using Evolutionary Algorithms: An Introduction," in *Multi-objective evolutionary optimisation for product design and manufacturing*, London, Springer, 2011, pp. 3-34.
- [62] J. Blank and K. Deb, "A Running Performance Metric and Termination Criterion for Evaluating Evolutionary Multi- and Many-objective Optimization Algorithm," in *2020 IEEE Congress on Evolutionary Computation (CEC)*, Glasgow, UK, 2020.